2298–2318 *Nucleic Acids Research, 2023, Vol. 51, No. 5* *Published online 21 February 2023*
https://doi.org/10.1093/nar/gkad085

The importance of nuclear RAGE–Mcm2 axis in diabetes or cancer-associated replication stress

Zhe Han[1], Martin Andrš[2,3], Bindhu K. Madhavan[1], Serap Kaymak[1], Alba Sulaj[1,6], Zoltan Kender[1,6], Stefan Kopf[1,6], Lars Kihm[1], Rainer Pepperkok[5], Pavel Janscak[2,3], Peter Nawroth[1,4,6,*] and Varun Kumar[1,4,5,6,*]

[1]Department of Medicine I and Clinical Chemistry, University Hospital of Heidelberg, INF 410, Heidelberg, Germany, [2]Institute of Molecular Genetics, Academy of Sciences of the Czech Republic, CZ-14300 Prague, Czech Republic, [3]Institute of Molecular Cancer Research, University of Zurich, 8057 Zurich, Switzerland, [4]Institute for Immunology, University Hospital of Heidelberg, INF 305, Heidelberg, Germany, [5]European Molecular Biology Laboratory, Advanced Light Microscopy Facility, Heidelberg, Germany and [6]German Center of Diabetes Research (DZD), Neuherberg, Germany

Received April 01, 2022; Revised January 18, 2023; Editorial Decision January 19, 2023; Accepted January 26, 2023

ABSTRACT

An elevated frequency of DNA replication defects is associated with diabetes and cancer. However, data linking these nuclear perturbations to the onset or progression of organ complications remained unexplored. Here, we report that RAGE (Receptor for Advanced Glycated Endproducts), previously believed to be an extracellular receptor, upon metabolic stress localizes to the damaged forks. There it interacts and stabilizes the minichromosome-maintenance (Mcm2–7) complex. Accordingly, RAGE deficiency leads to slowed fork progression, premature fork collapse, hypersensitivity to replication stress agents and reduction of viability, which was reversed by the reconstitution of RAGE. This was marked by the 53BP1/OPT-domain expression and the presence of micronuclei, premature loss-of-ciliated zones, increased incidences of tubular-karyomegaly, and finally, interstitial fibrosis. More importantly, the RAGE–Mcm2 axis was selectively compromised in cells expressing micronuclei in human biopsies and mouse models of diabetic nephropathy and cancer. Thus, the functional RAGE–Mcm2/7 axis is critical in handling replication stress *in vitro* and human disease.

GRAPHICAL ABSTRACT

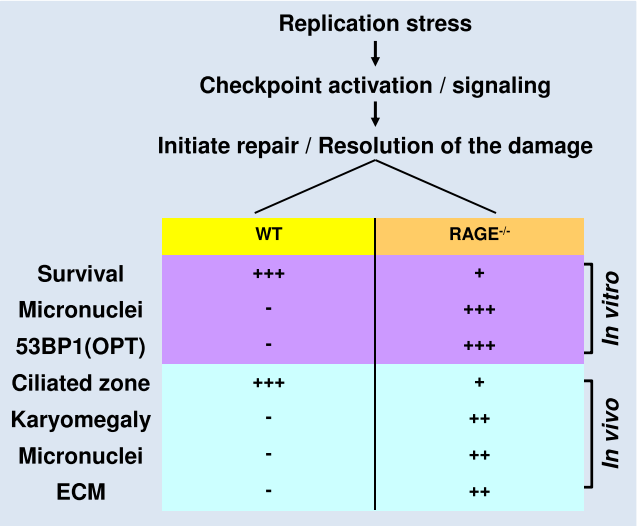

INTRODUCTION

DNA replication is a complex process that enables timely and accurate duplication of genetic information (1). Initiation of DNA replication is achieved through two sequential steps: origin licensing and origin firing (2). The origin licensing involves the systematic assembly of the inactive hexameric minichromosome maintenance (Mcm2–7) helicase complex at replication origins. This occurs during the M- and next G1-phase of the cell cycle. The conversion of this inactive Mcm2–7 complex to a functional

*To whom correspondence should be addressed. Tel: +49 6221 56 6970; Email: varun.kumar@med.uni-heidelberg.de
Correspondence may also be addressed to Peter Nawroth. Email: peter.nawroth@med.uni-heidelberg.de

replisome occurs during S-phase and is termed origin firing (3,4).

Further, depending upon the situation and cellular microenvironment, various impediments such as abnormal DNA structure, common fragile sites, DNA–protein crosslinks, and other DNA lesions collectively affect the faithful progression of the replication fork, commonly called fork stalling (5). However, in response to these hindrances, cells execute a series of regulated responses to stabilize the replisome structure, activate the checkpoint signaling, remove the cause of stalling, and reinitiate replication *via* the replication fork restart program (5). More importantly, this fork repair response is initiated by activating the ATR (ATM and Rad3-related)/CHK1 signaling axis. It cumulatively leads to the recruitment of repair factors to the stalled fork to remove the hindering perturbations and restart replication (6). Failure of the ATR response ultimately leads to replication fork collapse mediated through the ubiquitination of the replisome machinery, premature unloading of the clamp complex and cleavage of the DNA helix (7–9). Mcm2 serves as a downstream target of ATR signaling, to promote faithful progression of the replication fork (10). This points to the key role of stabilizing the Mcm complex, but the mechanisms stabilizing Mcm2–7 and maintaining its function during replication stress remain unknown.

The receptor for advanced glycation end-products (RAGE) is a multi-ligand receptor localizing to various organelles such as the nucleus, mitochondria, cytoplasm and cell membrane. It binds to multiple ligands such as advanced glycation end-products (AGEs), S100 protein family members, glycosaminoglycans, amyloid β-peptides, high-mobility group box-1 (HMGB1), double-stranded DNA and others (11). Previous work on nuclear RAGE has shown that upon induction of DNA double-strand breaks (DSBs), RAGE is recruited to the sites of damage *via* an ATM signaling cascade, and the absence of RAGE affects the ATR/Chk1 signaling (12–15). In addition, $RAGE^{-/-}$ cells show proliferation defects and massive endogenous damage compared to controls. However, the underlying causes of these defects are still unknown, albeit the phenotypic description of RAGE-deficient cells might be compatible with a loss of Mcm functions. To extend these observations to a broader base, the role of RAGE in replication stress and especially its interaction with Mcm2/7 was studied *in vitro* and *in vivo*.

In this study, we demonstrate that within a replication stress environment, RAGE interacts with Mcm2 and 7, and stabilizes the replication helicase complex, to promote faithful progression of the replication forks, thereby preventing the formation of micronuclei and the expression of 53BP1 in OPT domains and improves survivability. Congruently, the absence of RAGE increases the incidence of replication fork stalling and leads to the accumulation of extracellular matrix ECM components and the premature loss of ciliated cells in the kidney in stress situations. Thus, the nuclear RAGE–Mcm axis is essential for maintaining the synchrony of high cell turnover organs by participating in replication stress response.

MATERIALS AND METHODS

Cell culture and transfection

HEK293T, HeLa, U2OS, murine lung fibroblasts and U2OS-Lac*O* cells were grown in the DMEM medium (Life Technologies) described earlier (13,14). The isolation of primary murine lung fibroblasts from wild-type (WT) and $RAGE^{-/-}$ murine lungs was performed as described earlier (12). The generation and culture conditions for the *U2OS-LacO* cell line containing lac operator (*LacO*) were described elsewhere (16). Detailed information about the Hela $RAGE^{-/-}$cells generated by the CRISPR-Cas9 method is described earlier (14,17). The plasmid DNA transfection in HeLa, U2OS, U2OS-Lac*O*, HEK293T cells, or murine lung fibroblasts was performed using the TurboFect™ Transfection Reagent (Thermo Scientific). siRNAs were transfected into cells using Lipofectamine RNAi MAX (Invitrogen). Transfected cells were analyzed after 24–48 h of transfection.

Primary fibroblast culture

The isolation of primary murine lung fibroblasts from Wild type (WT) and $RAGE^{-/-}$ murine lungs was performed as described earlier (12).

Cell lysis, immunoprecipitation, and immunoblotting

Total cell extracts were obtained by resuspending them in ice-cold lysis buffer (20 mM Tris–Cl pH 7.5, 40 mM NaCl, 2 mM $MgCl_2$, 0.5% NP40, 50 U/ml Benzonase), with protease and phosphatase inhibitors, followed by adjustment of NaCl concentration to 150/450 mM. For immunoprecipitation of the various complexes, lysates were prepared from HEK293T cells that were transfected as indicated. Immunoprecipitation was then performed using the RFP-Trap Magnetic Agarose (ChromoTek) following the manufacturer's instructions. The clarified lysate or the immunoprecipitated complexes were resolved by 4–20% sodium dodecyl sulphate (SDS)-PAGE, transferred onto nitrocellulose and probed using the indicated antibodies (Table 4).

Antibodies, plasmids and serum details

Details of antibodies used in this study are described in Table 4. The sequences for the RAGE of murine or human origin represents the following accession numbers NP_031451.2, and NP_001193865.1 respectively on the NCBI database. The details of the oligos used for mutagenesis are described in Table 5. The fetal calf serum was purchased from Sigma (Cat# Sigma-Aldrich: F4135; Batch number 20H250).

Silver staining

Silver staining of the polyacrylamide gel was performed per the method described elsewhere (18).

Cellular immunofluorescence (IF)

Cells growing on poly L-lysine coated coverslips were stained as earlier described (14); if stated, cells were pre-extracted with CSK buffer for 1–2 min at room temperature. Samples were blocked in 5% bovine serum albumin and immune-stained using the indicated primary and secondary antibodies. Stained coverslips were mounted using Vectashield (Vector Laboratories) and observed on a Nikon A1R confocal microscope using a 60× objective. Images were further processed using ImageJ (Fiji). The analysis of micronuclei was performed by using the indicated specimens stained with alone DAPI, and the quantification of micronucleated cells was performed as described elsewhere (19).

In situ proximity ligation assay

Proximity ligation assay (PLA) was performed using the Duolink PLA kit (Sigma-Aldrich) following the manufacturer's instructions. Finally, coverslips were mounted using ProLong Gold antifade mounting medium. Images were acquired with an Olympus FV1200 confocal microscope (63×/1.40 oil immersion) and analyzed using ImageJ.

Immunofluorescence of tissue sections

Immunofluorescence staining of tissue sections was performed using the earlier reported method (12,20). Antigen retrieval was performed in retrieval buffer-A (10 mM Tris–Cl pH-9.0, 1 mM EDTA.0.05% Tween 20) for 20 min at 24°C. Fluorochrome conjugated and species adsorbed respected secondary antibodies were then used to detect the signal. The imaging of these sections was performed similarly to the method of cellular immunofluorescence staining.

Laser micro-irradiation

Laser irradiation of the indicated cells was performed using the method described earlier (12,15). In brief, cells were plated on glass-bottom dishes, pre-sensitized with 10 μM 5-bromo-2'-deoxyuridine (BrdU, Sigma-Aldrich, Taufkirchen, Germany) in phenol red-free medium (Gibco/Thermo GmbH, Darmstadt, Germany) for 24 h at 37°C. Micro-irradiation was performed with a FluoView1200 confocal microscope following the setting described previously (12,15).

Human control or SCLC biopsies

The control and SCLC array were purchased from Pantomics inc. USA (LC10010d, https://www.biomax.us/tissue-arrays/Lung/LC10010d) and stained as described in the respective section.

DNA fibre spreading assay

DNA fiber spreading assay was performed by the method described earlier (21). In brief, cells were labelled with 30 μM 5-chloro-2-deoxyuridine (CldU) for 30 min, washed three times with 1× PBS, and then labelled with 250 μM 5-iodo-2-deoxyuridine (IdU) for 30 min. For replication restart assay, cells were labelled with 30 μM 5-chloro-2-deoxyuridine (CldU) for 30 min, washed three times with 1× PBS, treated with 2 mM HU fork 2 h, washed three times with 1× PBS, and then labelled with 250 μM 5-Iodo-2-deoxyuridine (IdU) for 30 min. After labelling, cells were harvested by trypsinization and resuspended in PBS (2.5×10^5 cells/ml). About 2.5 μl of this cell suspension was mixed with 7.5 μl of lysis buffer [200 mM Tris–HCl (pH 7.5), 50 mM EDTA, 0.5% (w/v) SDS] on a glass slide by gently stirring with a pipette tip. After 9-min incubation at RT, the slides were tilted at 30–40°, the surface tension of the drops was disrupted by a tip, and the drops were allowed to glide down the slides slowly. The DNA spreads were air-dried and fixed in methanol/acetic acid (3:1) at 4°C overnight. DNA fibres were denatured with 2.5 M HCl for 1 h at RT, washed four times with 1× PBS and blocked with 2% BSA in 1× PBS for 40 min. After blocking, slides were incubated for 2 h in the dark at RT with rat monoclonal anti-BrdU antibody (ab6326, Abcam; 1:500 dilution) to detect CldU and mouse monoclonal anti-BrdU Antibody (347580, BD Biosciences; 1:100 dilution) to detect IdU. Slides were then washed four times with 1× PBST (PBS supplemented with 0.2% Tween-20) and incubated with secondary antibodies, donkey anti-rat Cy3 (712-166-153, Jackson Immunoresearch; 1:150 dilution) and goat anti-mouse Alexa 488 (A110334, Thermo Fisher Scientific; 1:300 dilution), for 1 hour in the dark at RT. After washing four times with 1× PBST, the slides were air-dried in the dark for 40 min at RT and mounted with ProLong Gold antifade mounting medium (25 ml/coverslip 24 × 50 mm). Images were acquired with a Leica DM6B upright fluorescent microscope (63×/1.40 oil immersion). CldU and IdU tract lengths (μm) were measured by using the segmented line tool of ImageJ.

Colony formation assay

HeLa WT and $RAGE^{-/-}$ cells were either left untreated or stimulated with hydroxyurea (HU) or glyoxal for 4 h. About 500 cells per well in six-well plates were seeded and incubated for colony formation. After 10 days, colonies were stained with 0.5% Crystal Violet (Sigma) for 20 min. The colonies were counted with OpenCFU (colony counting software). The percentage survival was calculated by normalizing the data with untreated (100%) ($RAGE^{+/+}$ or $RAGE^{-/-}$) cells.

Expression and purification of recombinant proteins

The pET28a-RAGE and GST-Mcm2 constructs were transformed into *Escherichia coli* BL21 (DE3) codon plus (Novagen) competent cells. The bacteria were cultured in LB or TB medium with vigorous shaking (200 rpm) at 37°C to a density of $OD_{600} = 0.8$ and then transferred to 25°C and induced with IPTG (0.4mM in water). Cultures were further incubated at the same conditions for 8 h. After induction, the cell culture was centrifuged at 6000 rpm for 15 min at 4°C. The cell pellet was frozen at –80°C for later use. The purification of the recombinant proteins was done using Ni-NTA and GST beads using QIA-expressionist method, and

the eluted protein was analyzed on SDS PAGE. The pure fractions collected were dialyzed in 1× PBS or indicated reaction buffer at 4°C overnight.

GST pulldown assay

GST pulldown assay was performed by using the method described elsewhere (22). In brief, 2 μg of the $(His)_6$-tagged RAGE, mixed with either 2 μg of GST-Mcm2 or GST alone in the pulldown buffer (2× buffer: 20 mM Tris–HCl, pH 7.9, 20% Glycerol, 10 mM $MgCl_2$, 300 mM KCl, 0.2% NP40, 30 mM imidazole, 1 mM PMSF and phosphatase inhibitors) along with glutathione agarose resin (Sigma). After 3 h of incubation, the beads were extensively washed in the pulldown buffer. The proteins were then extracted from the beads into the SDS sample buffer and probed with appropriate antibodies.

Cycloheximide based protein stability assay

The cycloheximide-based protein stability assay was performed using the method described elsewhere (23). In brief, cells were transfected with the indicated constructs. After 36 h of transfection, cells were simultaneously treated with replication stress agent hydroxyurea (HU; 2 mM for 4 h) and cycloheximide (in water; 0.25 mM). After 4 h of replication stress, the medium was replaced with a fresh medium containing only cycloheximide (CHX). A fraction of the cells was collected at the 0-h time point, and the subsequent time points were collected at the indicated time intervals. These samples were then analyzed by immunoblotting using indicated antibodies.

Preparation of peripheral blood mononuclear cells and cytospin

Peripheral blood mononuclear cells (PBMCs) were separated from the whole blood using the method described elsewhere (24,25). Prepared PBMCs were suspended in PBS and gently cytospun on the glass slides. The sample smear was fixed (4% PFA 10 min at RT) and stained as described in H&E staining section.

H&E staining

The processed sections were stained with hematoxylin for about 10 min (30 °C), water rinsed for 15 min and then differentiated in acid solution by incubating them for 5–30 s until the slice got red, then rinsed with water. These sections were then placed into 75%, 95% and l00% ethanol solution for 5 min each and then eosin dye staining was performed for about 2 min. The eosin-stained sections were sequentially dehydrated for 5 min each and then placed into the xylene-I and xylene-II solution each for 5 min. The slides were mounted in the mounting medium and dried overnight before analyzing them under a microscope. The evaluation and the analysis of tubular karyomegaly were performed as described elsewhere (26).

Trichrome masson staining

Staining was performed on renal sections by following the method described earlier (12,13).

Mouse models

All the experimental procedures were carried out in two different mouse strains: The wild type (WT) and $RAGE^{-/-}$ generated in *C57BL6* and *SV129* background (27). The animal care and use committees approved the experiments' procedure at the Regierungsspräsidium Tübingen and Karlsruhe, Germany (G-90 and G-182). The STZ mice were considered diabetic if blood glucose levels were above 300 mg/dl 16 days after the last STZ injection, as described earlier (13). Blood and tissue samples were obtained after the indicated periods described in the result section.

Ethics statement on patient samples

All experiments were conducted following the Declaration of Helsinki and the International Ethical Guidelines for Biomedical Research Involving Human Subjects. The local ethics committee approved the study (ethics board approval S-206/2005, S270/2018 and S-284/2018). Formalin-fixed and paraffin-embedded tissue samples were cut into 3 μm thick sections and put on glass slides.

Graph plotting and statistical analysis

Prism (version 8.0.1, GraphPad) was used to perform the statistical analysis. Significance was expressed as P values (ns, $P > 0.5$; $*P < 0.05$, $**P < 0.01$, $***P < 0.001$ and $****P < 0.0001$). For the comparison of the two groups, unpaired two-tailed t-test was used. When more than two groups were analyzed, one-way ANOVA was performed, followed by Tukey's test. To determine the statistical differences between genotypes at different time points or different concentrations, two-way ANOVA with Sidak's test was performed. At least three independent biological replicates were used. Mann-Whitney nonparametric test was used to compare replication tract lengths and asymmetry from DNA fiber assay. Colocalization analyses were carried out using JACoP plugin (28). Manders' colocalization coefficient (29), and Pearson's correlation coefficient (30) were used to quantify colocalization.

RESULTS

Identification of DNA replication licensing factor Mcm2 as an interacting partner of nuclear RAGE

RAGE constitutively localizes in the nucleus of mammalian cells. Recently we have elucidated that nuclear RAGE (nRAGE) participates in DNA DSBs repair; however, irrespective of the DSBs, its constitutive localization in the nucleus indicates other functions (12–15). $RAGE^{-/-}$ cells show proliferation defects and an increased frequency of micronuclei, a phenotype compatible with replication defects. Therefore potential RAGE interacting partners were studied under basal and hydroxyurea-induced replication stress. A coupled strategy involving hydroxyurea (HU) treatment, followed by immunoprecipitation and LC-MS/MS-based identification, was used (Figure 1A). From nuclear extracts of HU-treated HEK293T cells, RAGE retrieved a wide range of interacting proteins. Among these, 135, 80, 40, 34 and 20 kDa bands were more prominent than

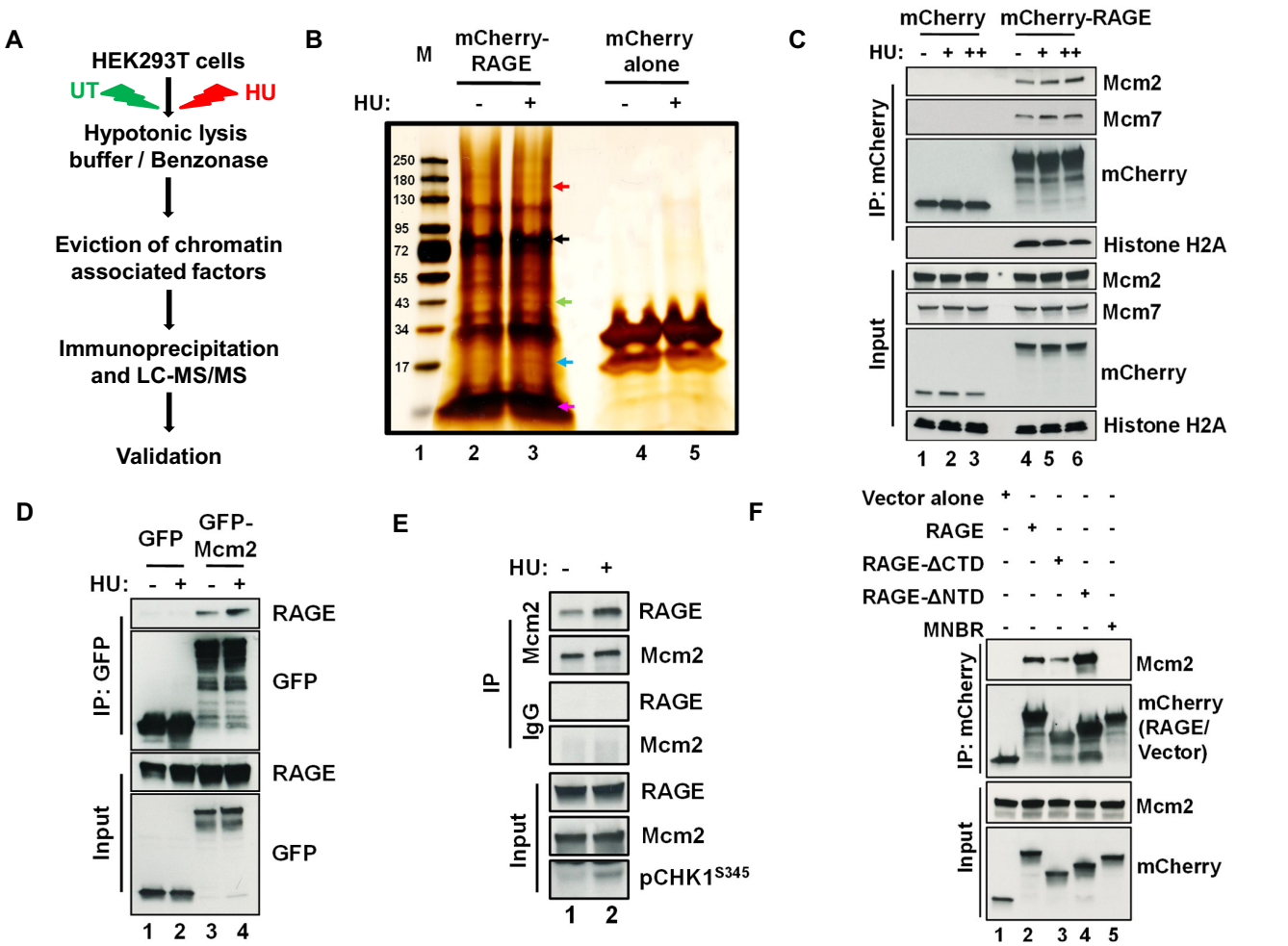

Figure 1. Nuclear RAGE interacts with the DNA replication helicase complex subunits Mcm2/7. (**A**) Schematic representation of the steps used for identifying the interacting partners of RAGE in the nucleus from HEK293T cells left untreated (UT) or treated with the replication stress agent hydroxyurea (HU; 2 mM for 4 h). (**B**) Silver-stained gel showing the proteins retrieved from the mCherry trap beads by using the lysate of untreated (–) or hydroxyurea treated (+; HU 2 mM for 4 h) HEK293T cells ectopically expressing either mCherry-RAGE or mCherry alone. Mcm2 and Mcm7 were identified by LC-MS/MS, marked by a red and black arrow, respectively. The label M indicates a protein marker. (**C**) Co-immunoprecipitation blots showing the interaction of RAGE with the replication helicase complex (as represented by Mcm2/Mcm7). Co-immunoprecipitation was performed from the lysate of control (–) or HU (+ represents 200μM, ++ represents 2 mM; for 4 h) treated HEK293T cells over-expressing either mCherry-hRAGE or mCherry alone. (**D**) Representative immunoblots showing the replication stress-induced RAGE–Mcm2 interaction. Co-immunoprecipitation was performed using mCherry trap beads from the lysate of control (–) or HU (+) (2 mM; 4 h) treated HEK293T cells over-expressing either mCherry-hRAGE and EGFP-Mcm2, or mCherry-hRAGE and alone GFP. (**E**) Co-immunoprecipitation immunoblots showing the RAGE–Mcm2 interaction from the lysate of control (–) or HU (+) (2 mM; 4 h) treated HEK293T cells ectopically expressing mCherry-hRAGE with anti-Mcm2 or IgG control. pCHK1 S345 served as the control to verify the activation of replication stress signaling. (**F**) HEK293T cells ectopically expressing either mCherry vector (lane 1), full-length mCherry-RAGE (lane 2) or mCherry-RAGE deletion constructs (lanes 3, 4 and 5) were treated with HU (2 mM, 4 h). Here FL represents full-length, ΔNTD/ΔCTD represents the deletion of the N- or C-terminal domain of RAGE, and MNBR represents the Mcm2 non-binding mutant of RAGE.

others (Figure 1B). Mass spectrometry analysis showed that RAGE interacts with the miniature chromosome maintenance complex subunits (Mcm) 2 and 7 (Table 1). More importantly, this RAGE/Mcm interaction was markedly enhanced in cells treated with replication stress-inducing agent HU (Figure 1B). The LC-MS/MS data were verified using the HEK293T cells expressing mCherry-RAGE or mCherry alone. These cells were either left untreated or treated with either a low (200 μM; 4 h) or a high (2 mM; 4 h) concentration of HU, known to activate checkpoint signaling (Supplementary Figure 1A). Co-immunoprecipitation data show that nuclear RAGE interacts with the Mcm complex subunits 2 and 7. This interaction was enhanced upon HU treatment (Figure 1C; lane 4 versus lane 5 or 6).

In contrast, the interaction with core histones remained unchanged under these situations (Figure 1C, lane 4 versus lane 5 or 6). Further, mCherry alone showed no interaction with either the Mcm2 or the Mcm7 subunit of replication helicase under these conditions (Figure 1C, lanes 1–3). In proliferating cells, Mcm subunits can exist in two forms; in one, it exists as a free factor, whereas in another, it assembles into an active replication helicase complex. However, considering that two different subunits of the replication helicase, i.e. Mcm2 and Mcm7, were detected in RAGE

Table 1. A list of RAGE associated protein under untreated (–) or Hydroxyurea (HU; +) treated condition

Treatment	–	+
Protein↓	No. of peptides in RAGE IP	
Mcm2	23	73
Mcm7	11	46
RPA2	23	47
H2AX	8	22
RANGAP1	1	5
RBBP4	3	9
PCNA	2	13

immunoprecipitation, it suggests that RAGE interacts with assembled Mcm complex.

To further confirm these co-immunoprecipitation data, a reciprocal immunoprecipitation was performed by using the HEK293T cells expressing GFP-Mcm2 and mCherry-RAGE. Immunoprecipitation of GFP-tagged Mcm2 also co-immunoprecipitated RAGE, and this interaction was markedly enhanced in HU-treated cells (Figure 1D lane 3 *vs* lane 4). In contrast, GFP alone showed no interaction with RAGE or Mcm complex in basal or replication stress situations (Figure 1D, lane 1 versus lane 2). Similar to the GFP-tagged Mcm2, immunoprecipitation of endogenous Mcm2 from the cells either left untreated (–) or were treated with HU (+) also co-immunoprecipitated RAGE in a manner that depends on the HU stimulation (Figure 1E, lane 1 versus lane 2, as marked by the Chk1 phosphorylation; $pCHK1^{S345}$). These data show that nuclear RAGE interacts with Mcm2, and this interaction is modulated by HU treatment.

Since RAGE and Mcm2/7 are chromatin-interacting proteins, the observed interaction might be mediated through DNA. To clarify this, two independent approaches were used. First, we used ethidium bromide (EtBr) to disrupt any DNA-protein interactions in the lysate used for immunoprecipitation. A more direct protein pulldown assay was utilized in the second approach. EtBr-treatment of the lysate neither affected nor disrupted the RAGE/Mcm2 interaction (Supplementary Figure 1B, lane 2 versus lane 3), indicating that the RAGE–Mcm2 interaction is likely mediated *via* direct protein-protein interaction but not *via* DNA. To confirm this further, a GST pulldown assay was performed using the purified GST-tagged Mcm2 (bait) and the $(His)_6$-tagged RAGE (prey) (Supplementary Figure 1C). The pulldown assay showed that GST-tagged Mcm2 could capture the $(His)_6$-tagged RAGE (Supplementary Figure 1D, lane 4). In contrast, GST alone showed no such interaction with RAGE under similar conditions, indicating this assay's specificity (Supplementary Figure 1D, lane 5). Cumulatively, this indicates that RAGE interacts with Mcm2 through direct protein-protein interaction.

The N-terminus of RAGE contains an SAP domain with an AT-hook, whereas the C-terminus of RAGE harbours the signaling and DNA binding modules. To understand the importance of these modules in the RAGE/Mcm2 interaction, extensive *in silico* structure modelling tools were utilized. These data predicted that RAGE encircles the Mcm2 complex using the conserved amino acid residues from the far N-terminus and the C-terminus signaling module. More importantly, our prediction also showed that this RAGE/Mcm2 interaction interface is distinct from the RAGE/MRE11 interface. To test this prediction, we generated a mutant with a lysine mutation (K173A) closer to the AT-hook motif located at the N-terminus and a deletion of a stretch of 13 amino acids (residues from 309–322 of human RAGE). This RAGE construct was labeled as an **M**cm2 **N**on-**B**inding mutant of **R**AGE (MNBR) (Supplementary Figure 2A). From the *in silico* analysis, it was predicted that these mutations abolished the RAGE/Mcm2 interaction needed in response to replication stress. MNBR and the other RAGE deletions were studied in comparison with full-length RAGE in the co-immunoprecipitation assay (Supplementary Figure 2A). mCherry alone served as a negative control of the immunoprecipitation. Upon replication stress, full-length RAGE, N-terminus deleted domain (ΔNTD), and the C-terminus deleted domain (ΔCTD) of RAGE interacted with Mcm2 (Figure 1F, lanes 2–4).

Interestingly, the ΔNTD mutant of RAGE enhanced the RAGE/Mcm2 interaction, indicating that the deleted region might negatively regulate the RAGE/Mcm2 interaction. Contrary to the full-length and other RAGE deletions, neither the MNBR mutant nor the mCherry alone could bind to the Mcm2 in a replication stress situation (Figure 1F, lanes 2, 3 and 4 versus 1 or 5), supporting the result of the in silico analysis. This indicates that both the N-terminus and C-terminus region of the nuclear RAGE play a vital role in RAGE/Mcm2 interaction, and MNBR mutation blocks this interaction completely.

Further, to test if amino acid changes in MNBR indeed makes this RAGE mutant specifically deficient for its interaction with Mcm2, but not other nuclear function of RAGE such as MRE11 binding dependent DNA DSBs repair in the nucleus (12,15), laser-induced DNA DSBs recruitment studies were performed by using either the mCherry-tagged full-length or the MNBR-RAGE in conjunction with GFP-Nbs1. Like full-length RAGE, MNBR can also recruit to the site of DNA damage (Supplementary Figure 2B; left versus right panels). This shows that the MNBR mutation does not affect the DNA DSBs repair function of the nuclear RAGE but specifically abolishes the functional RAGE/Mcm2 axis.

In the above IP experiments, we have used HEK293T cells with the RAGE and Mcm2 of human origin. To rule out any cell type or species dependency of this interaction, the immunoprecipitation was repeated in Hela and U2OS cells. Like the HEK293T cells, immunoprecipitation from Hela (Supplementary Figure 2C) or U2OS (Supplementary Figure 2D) cells also showed that RAGE interacts with Mcm2. As expected, this interaction was enhanced by HU treatment. Further, to exclude the species dependency in RAGE/Mcm2 interaction, either full-length RAGE or the cytoplasmic domain of murine RAGE (not capable of entering the nucleus (12) was studied. Immunoprecipitation with murine RAGE also showed that full-length RAGE, but not the cytoplasmic RAGE or the GFP alone, interact with the Mcm2 (Supplementary Figure 2E, lane 2 versus lane 1 or 3). Collectively, these data show that irrespective of the cell-type or species of RAGE origin used, RAGE interacts with Mcm2 and this interaction is markedly enhanced by replication stress.

Replication stress modulates the timely association of RAGE with the Mcm2 complex

To gain insight into how the RAGE–Mcm2/7 axis might contribute to genomic stability, the replication stress response was studied in U2OS cells. To induce the replication stress, two independent agents were used. Hydroxyurea (HU) induces a deoxynucleotide imbalance and activates the replication stress response (31). Also, glyoxal, an alternative replication stress-inducing agent which affects replisome progression and thus induces replication stress (32) in metabolic disease and cancer, was used. After HU treatment, RAGE colocalizes with the replication helicase complex subunits Mcm2 (Figure 2A; left panel and Supplementary Figure 3A; upper panels; $P < 0.01$; $n = 2$) and Mcm7 (Figure 2A; right panel and Supplementary Figure 3A; lower panels; $P < 0.001$; $n = 2$).

RAGE in the nucleus exists in two forms, a chromatin-bound form that performs the chromatin-associated functions (12,33) and another nucleoplasmic form which is freely available for chromatin-dependent or independent functions of RAGE in the nucleus (33). Thus, to prevent colocalization interferences from the nucleoplasmic form, the **P**roximity **L**igation **A**ssay (PLA) and the lacO system (16) were utilized in parallel. At first, U2OS cells ectopically expressing FLAG tagged-RAGE were studied in PLA. PLA signal confirmed that upon HU treatment, RAGE and Mcm2 were in very close vicinity to activate the proximity ligation system; in contrast, neither Mcm2 nor the FLAG antibody alone showed any signal, thus validating the specificity of this assay (Figure 2B, Supplementary Figure 3B). In the second approach, U2OS-lac*O* cells ectopically expressing EGFP-tagged-Mcm2 in conjunction with either Lac*I*-mCherry or Lac*I*-mCherry-RAGE were used (Figure 2C). HU treatment also promotes the enrichment of Mcm2 onto the immobilized RAGE, as observed by the native fluorescence of each fluorescent tag (Figure 2D and E), whereas, Lac*I*-mCherry itself showed a very weak or no binding (Figure 2D and E).

To further validate the importance of the RAGE–Mcm interaction in replication stress, immunoprecipitation, colocalization and PLA studies were repeated in the presence of glyoxal. Immunoprecipitation studies from HEK293T cells ectopically expressing mCherry-RAGE showed that glyoxal treatment (0.5 mM for 4 h) promotes the RAGE–Mcm2 interaction (Supplementary Figure 4A, lanes 1 and 2). In contrast, mCherry alone showed no interaction in either glyoxal-treated or untreated cells (Supplementary Figure 4A, lanes 3 and 4). Co-localization (Supplementary Figure 4B, C; $P < 0.01$; $n = 2$) and PLA (Figure 2F) also confirmed immunoprecipitation data that glyoxal promotes the RAGE–Mcm interaction in a manner comparable to HU. Thus, these data prove that both replication stress-inducing agents enable the association of nuclear RAGE with Mcm complex.

DNA damage and replication stress induce phase separation of the nuclear factors to form repair foci (34,35). RAGE forms visible repair foci at DSBs, which colocalize with the DNA end-resection complex (MRN) (12). Therefore, to test if replication stress promotes the accumulation of RAGE in visible foci, HU-mediated replication stress was performed in U2OS cells, expressing mCherry-tagged RAGE. After the indicated HU time intervals, these cells were detergent extracted (CSK; (14)), fixed, and the native mCherry fluorescence was then used for determining the pattern of RAGE. Upon HU treatment, RAGE forms visible foci, which became apparent after 20–30 min and were stable for a longer time (Supplementary Figure 5A).

RAGE is known to express in various organ systems (14). Since glyoxal, a replication stress-inducing agent, regulates the RAGE/Mcm2 or 7 interaction, the RAGE colocalization with Mcm2 was studied in tissue sections from murine diabetic lungs and human small cell lung carcinoma (SCLC) biopsies. After staining the tissue with RAGE and Mcm2 antibodies, the colocalization coefficient (Pearson's correlation) (R) was calculated (29,36). The data show that RAGE colocalizes with Mcm2 with an R-value of 0.862 in murine diabetic lungs (Supplementary Figure 5 B, C) and 0.924 for the human SCLC biopsies (Supplementary Figure 6). Altogether, these data demonstrate that RAGE colocalizes with Mcm2 in a murine model of diabetes and human cancer, further supporting the hypothesis, that this interaction might be of relevance.

RAGE protects cells from replication stress

Perturbed replication fork progression is associated with increased DNA damage and is the main culprit inducing replication stress. Previously we have shown that the absence of RAGE affects the proliferative potential of primary lung fibroblasts and that these cells accumulate endogenous DNA damage (12). To understand the importance of the RAGE–Mcm axis in replication stress response, Hela^{WT} and Hela RAGE$^{-/-}$ (RAGE$^{-/-}$) cells were exposed to various concentrations of HU or glyoxal and their post-replication stress recovery was determined in a colony-forming assay. To rule out non-specific genome editing of these cells, two independent Hela RAGE$^{-/-}$ clones (clone 1 and clone 2; 14) were studied in parallel to the Hela RAGE$^{+/+}$ cells. It was observed that RAGE$^{-/-}$ cells were more sensitive to replication stress at the various concentrations tested (Figure 3A, B; $P < 0.001$ to 0.0001; $n = 6$, and Supplementary Figure 7A; $P < 0.05$ to 0.0001; $n = 6$).

Further, to rule out the influence of cell type-specific effects, the post-replication stress survival potential of murine lung fibroblasts harvested from WT and RAGE$^{-/-}$ mice were also studied (27). Similar to the phenotype observed with Hela RAGE$^{-/-}$ cells, RAGE$^{-/-}$ lung fibroblasts were sensitive to HU (Supplementary Figure 7B, C; $P < 0.0001$; $n = 6$) or the glyoxal (Supplementary Figure 7D; $P < 0.01$; $n = 6$) concentrations tested, indicating an inherent function of RAGE in a replication stress situation.

To investigate the underlying mechanism, a single-molecule DNA fiber spreading analysis of replication fork progression was performed in WT and RAGE$^{-/-}$ cells. Cells were pulsed with chlorodeoxyuridine (CldU) for 30 min and then with iododeoxyuridine (IdU) for another 30 min. The double labeling with CldU and IdU allows the deep analysis of fork progression speed and the new origin firing. The replication fork progression speed was mildly decreased under basal conditions (Supplementary Figure 8A,

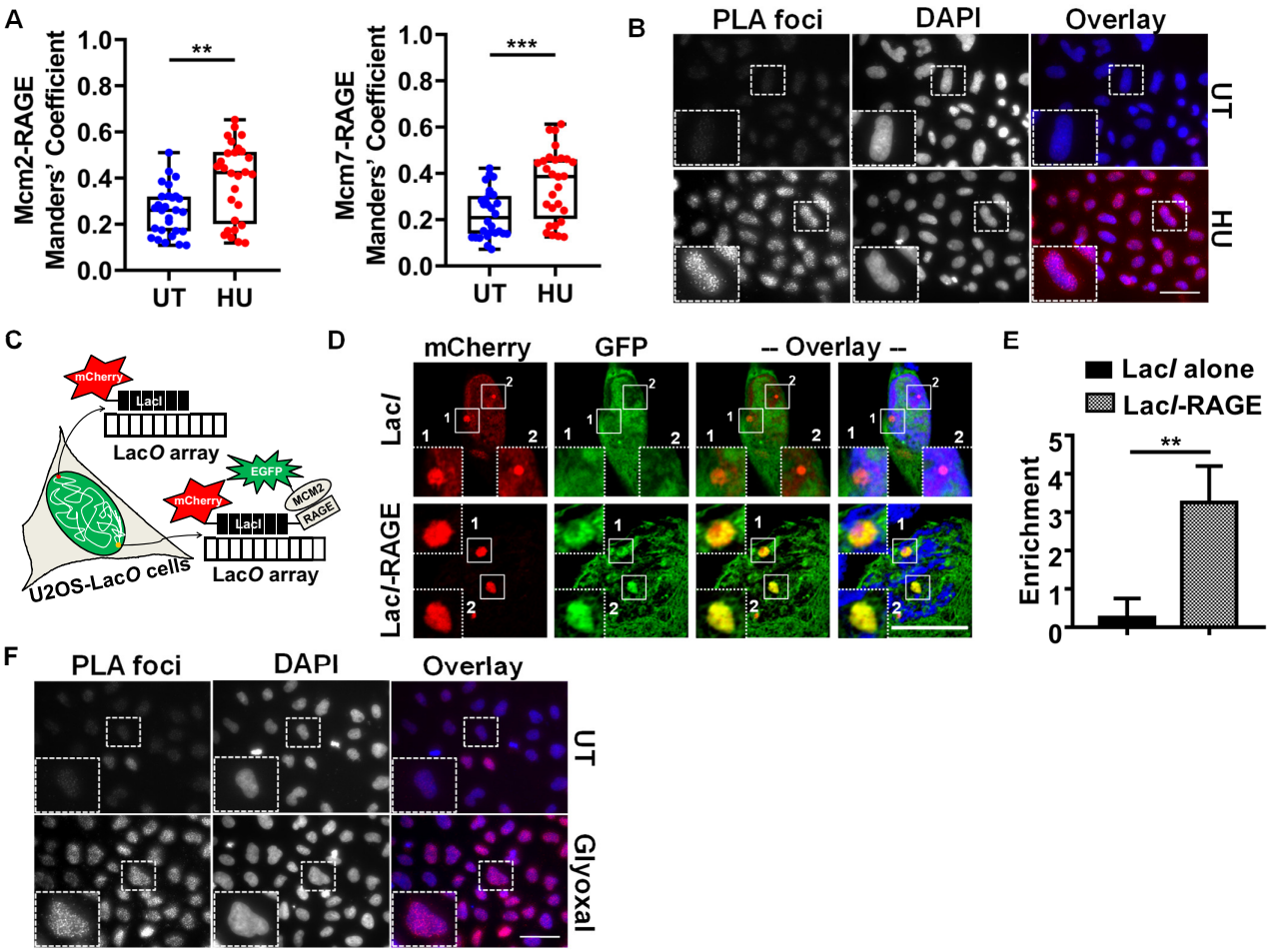

Figure 2. Replication stress promotes the recruitment of RAGE into the miniature-chromosome complex. (**A**) The quantitative analysis showing the Mander's colocalization coefficient for the RAGE/Mcm2 or RAGE/Mcm7 colocalization of the data presented in Supplementary Figure 3A. Data represents mean ± SEM, $^{**}P < 0.01$; $^{***}P < 0.001$, $n = 2$; >30 cells were analyzed for each condition. (**B**) Representative images showing the proximity ligation assay (PLA) signal in U2OS cells. These cells were ectopically expressing Flag-RAGE. Replication stress was induced by incubation with hydroxyurea (HU; 2 mM, 4 h), showing the replication stress-induced association of Mcm2 with RAGE, as marked by the PLA signal. The zoom window represents 3× magnification highlighted in dotted white boxes (scale 20 μm). (**C**) Schematic representation of the fluorescence-two-hybrid (F2H) system used for validating the stress-induced RAGE–Mcm2 interaction in U2OS cells (stably integrated with Lac*O* array) by using Lac*I*-mCherry-alone or Lac*I*-mCherry-RAGE (bait) and EGFP–Mcm2 (prey). (**D**) Representative images of U2OS-Lac*O* cells expressing the F2H system show that immobilization of RAGE onto the chromatin (bait) enriches Mcm2 (prey) onto the chromatin. The zoom window represents 2× magnification of the indicated areas, highlighted in dotted white boxes (scale 10 μm). (**E**) The quantitative analysis of the F2H data is shown in (D). Data represents mean ± SEM, $^{**}P < 0.01$; >50 cells were analyzed for each condition. (**F**) Representative images showing the proximity ligation assay (PLA) signal in U2OS cells. These cells were ectopically expressing Flag-RAGE. Stress was induced by incubating them with glyoxal (0.5 mM, 4 h), showing the association of Mcm2 with RAGE, marked by the PLA signal. The zoom window represents 3× magnification of the indicated areas, highlighted in dotted white boxes (scale 20 μm).

B and C, $P < 0.05$; $n = 3$) in the RAGE$^{-/-}$ cells. Typically, the replication forks move synchronically in a bi-directional manner unless the replication-cum-repair machinery of a cell has problems in faithful progression or restart of replication forks (21). Thus, measurement of the lengths of replication tracts of sister forks can be used to analyze the incidence of fork stalling. The progression of sister forks emanating from a common origin was studied by measuring the lengths of the halogenated DNA tracts (IdU) for each pair of the sister forks. The ratio of shorter to longer tract was calculated (sister fork ratio) and plotted for WT or RAGE$^{-/-}$ cells. In this assay, RAGE$^{-/-}$ cells had an increased frequency of asymmetric sister replication tracts (sister fork ratio much lower than 1), indicative of an inherent loss of fork stability or faithful progression ability (Figure 3C, D and Supplementary Figure 8D; $P < 0.0001$; $n = 3$). This data suggests that the absence of nuclear RAGE affects the normal progression of replication under replication stress situations.

The presence of RAGE might keep the fork replication proficient under basal conditions or after the replication stress or blockage has removed. To test this, a modified DNA fibre assay was performed by inducing the replication stress between the CldU and IdU pulses (Figure 3E)'. It was observed that in the absence of RAGE, the frequency of stalled replication forks is significantly enhanced under basal as well as after replication stress induction (Figure 3F, G; $P < 0.05$ (basal) or <0.01 (HU); $n = 4$).

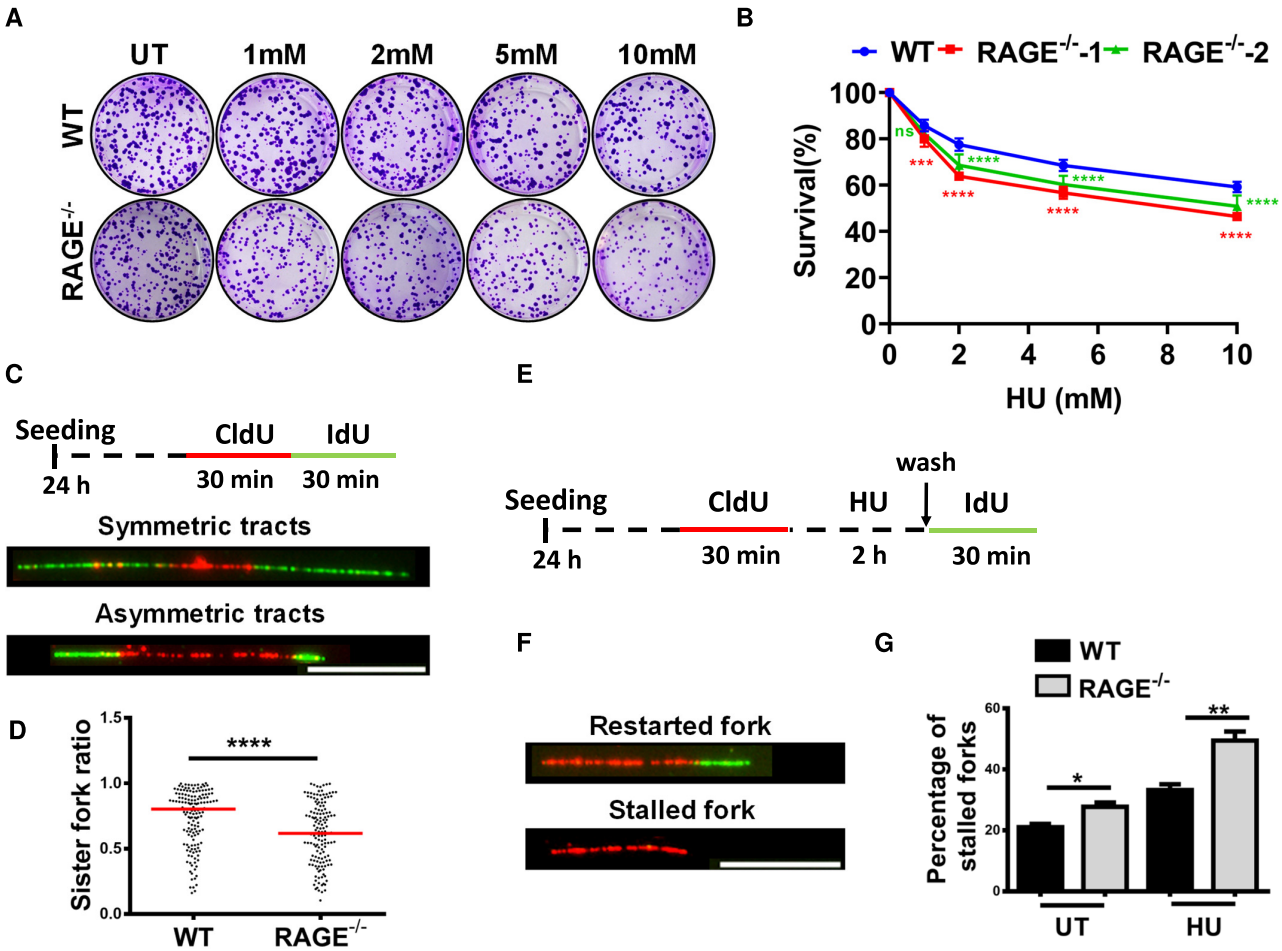

Figure 3. Absence of RAGE sensitizes the faithful progression of the replication fork under stress situation. (**A**) Representative images of the colonies from WT or RAGE$^{-/-}$ Hela cells either left untreated (UT) or treated with HU (indicated concentrations for 4 h), showing the percentage survival potential of these cells to recover from the HU-mediated replication stress. Colonies were stained after 10 days of recovery. (**B**) Quantitative analysis of the percentage survival potential of the indicated cells as described in (A). Two different Hela RAGE$^{-/-}$ clones were simultaneously studied. Data represented mean survival, ***$P < 0.001$, and ****$P < 0.0001$; $n = 6$. (**C**) Schematic preview and the representative images showing the pattern of symmetric and asymmetric sister forks observed in DNA fiber assay in WT or RAGE$^{-/-}$ Hela cells under basal conditions; scale bar, 10 μM. (**D**) Quantitative fiber spreading assay data showing the ratio of sister forks (shorter/longer) >50 tracts were scored for each data set, ****$P < 0.0001$; $n = 3$). The red bar indicates the median. Mann–Whitney nonparametric test was used to compare replication tract lengths and asymmetry from DNA fiber assay. (**E**) Schematic representation showing the plan of a modified DNA fiber assay. Here, the replication stress was induced between the pulses of CldU or IdU. (**F**) Representative images showing the pattern of stalled and restarted replication tracts observed in DNA fiber assay in WT or RAGE$^{-/-}$ Hela cells under HU treatment, scale bar, 10 μM. (**G**) Quantitative analysis of the fiber spreading data showing the percentage of stalled (CldU only) forks for the indicated conditions. >200 tracts were scored for each data set; *$P < 0.05$; **$P < 0.01$; $n = 4$.

RAGE supports the timely repair of replication progression defects

To examine the early or delayed post-replication stress defects induced by replication stress, WT and RAGE$^{-/-}$ cells were studied immediately after the indicated replication stress or after their re-entry into the next cell cycle (16 h) because cells cumulatively express all the unrepaired replication defects in the next cell cycle (37). Among these, the most important is the 53BP1 marked OPT domain in the G1-phase and the presence of micronuclei. In a comparative analysis of these two markers at early or later points in WT and RAGE$^{-/-}$ cells, it was observed that the absence of RAGE, particularly after replication stress, leads to a significant increase of single large OPT domains (pointed with yellow arrow), as marked by the absence of cyclin-A positivity (Figure 4A, B and Supplementary Figure 9A; $P < 0.05$–0.0001; $n = 2$), whereas control cells timely recover from this stress (Figure 4A, B). This was further validated by Chk1 (Chk1^{S345}) phosphorylation (Supplementary Figure 9B). Like HU-mediated replication stress, glyoxal-induced replication stress showed a markedly elevated frequency of 53BP1 expression in OPT-domains (Supplementary Figure 10A, B), further supporting the notion that the absence of RAGE during replication stress inhibits the timely resolution of replication perturbations.

Micronuclei are considered a well-defined marker for replication defects a cell might have encountered during the previous cell cycle phase (19). Therefore, to verify the 53BP1 data showing the compromised post-replication stress recovery of RAGE$^{-/-}$ cells, micronuclei frequency in WT and RAGE$^{-/-}$ cells was determined after 16 h of

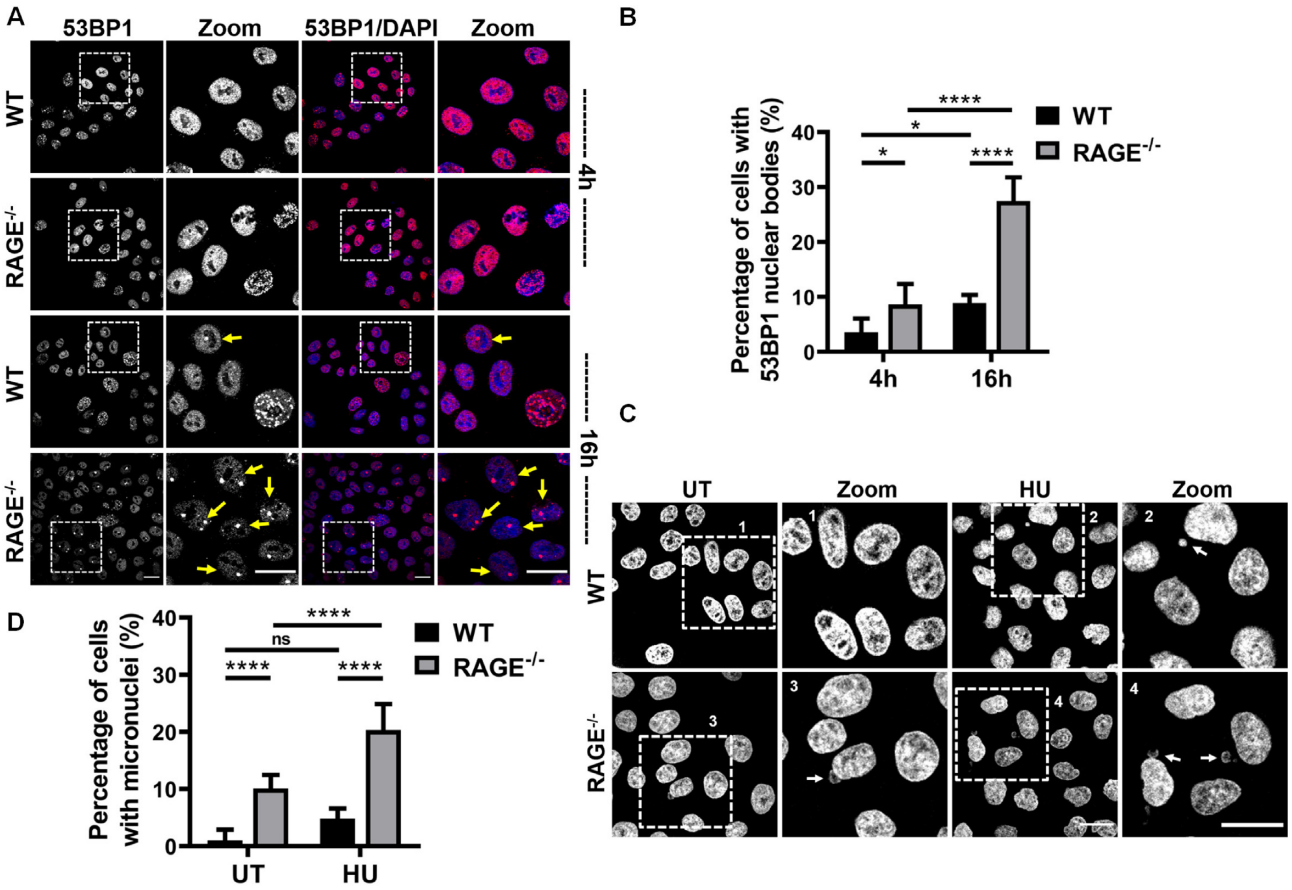

Figure 4. Under replication stress situations, RAGE prevents the expression of 53BP1 in OPT domain and the appearance of micronuclei. (**A**) Representative immunofluorescence images showing a comparative analysis of HU stress repair potential, as evidenced by single large 53BP1 foci, as marked by yellow arrowheads, in WT or RAGE$^{-/-}$ Hela cells at the indicated time points (4 hours:4 h, or 16 hours:16 h). The zoom window (in dotted white boxes) represents the respective zoomed areas (scale 25 μm). (**B**) Quantitative analysis of the post-replication stress repair potential of the WT or RAGE$^{-/-}$ cells described in (A). Data represented mean ± SD, *$P < 0.05$; ****$P < 0.0001$; $n = 2$; >500 cells were counted for each case. (**C**) Representative immunofluorescence images showing the micronuclei frequency in WT or RAGE$^{-/-}$ Hela cells after 24 h post-replication stress (HU, 2 mM for 4 h) chase. The white arrowhead points to micronuclei (scale 25 μm). (**D**) Quantitative analysis of the post-replication stress repair potential of WT or RAGE$^{-/-}$ cells shown in (C). Data represented as mean ± SD, ****$P < 0.0001$; $n = 3$; >250 cells were analyzed for each condition.

HU-mediated replication stress. The absence of RAGE significantly increases the frequency of micronuclei formation in untreated cells or 24 h after replication stress (Figure 4C, D; $P < 0.0001$; $n = 3$).

Further, to verify that this large clustering of 53BP1 in OPT domains is indeed associated with the absence of RAGE but not a Hela cell-specific observation, WT or RAGE$^{-/-}$ lung fibroblasts were studied in parallel to Hela cells. Similar to Hela cells, the absence of RAGE from lung fibroblasts markedly enhanced the clustering of 53BP1 in OPT domains (Supplementary Figure 11A, B; $P < 0.05$–0.0001; $n = 2$) and also increased the frequency of micronuclei in these cells (Supplementary Figure 12A, B; $P < 0.01$–0.0001; $n = 2$), indicating that absence of RAGE from Hela or lung fibroblasts express similar defects in the post-replication stress recovery phase. These data indicate that RAGE participates in maintaining the stability of the replication fork under stress situations since the absence of RAGE sensitizes the cells to endogenous or exogenous replication defects.

RAGE stabilizes the levels of Mcm2 in replication stress situations

Increased Mcm protein levels protect cells from replication stress-associated catastrophes (38). Further, the absence of nuclear RAGE makes the cells adversely sensitive to the two different replication stress agents tested. Therefore, we hypothesized that RAGE might stabilize Mcm2 and other components of the replication helicase complex, particularly under replication stress situations. To test this hypothesis, Hela RAGE$^{-/-}$ cells were either complemented with mCherry-RAGE or just mCherry expressing vector alone. After 36 h of transfection, these cells were co-treated with HU (2 mM for 4 h) and Cycloheximide (CHX; 0.25 mM), as shown in the scheme (Figure 5A). After 4 h of HU treatment, post-replication stress time points were collected under the constant pulse of CHX (Figure 5A). The collected samples were then analyzed for the stability of Mcm2 in cells expressing either mCherry alone or mCherry-RAGE. Under replication stress, Mcm2 levels in cells expressing mCherry alone decreased over time, indicating degradation of Mcm2. The presence of mCherry has no stabilizing ef-

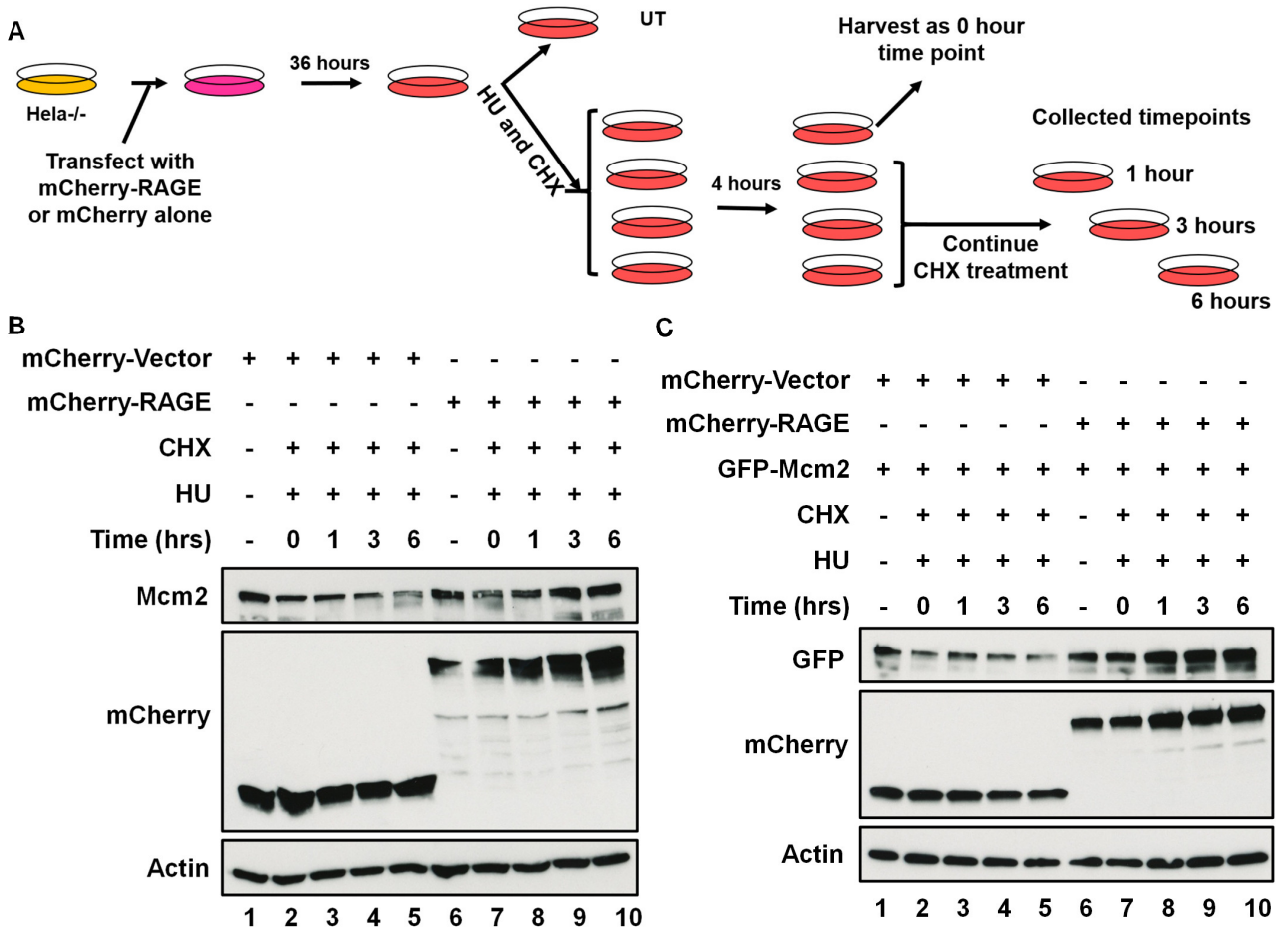

Figure 5. RAGE stabilizes the levels of Mcm2 under replication stress. (**A**) Schematic presentation of the steps involved in Cycloheximidine (CHX) pulse-chase experiment in Hela RAGE$^{-/-}$ cells transfected with a plasmid expressing mCherry alone or the mCherry-RAGE. The samples were collected at 0, 1, 3 and 6 h. (**B**) Representative immunoblots showing the levels of endogenous Mcm2 in Hela RAGE$^{-/-}$ cells expressing mCherry alone or mCherry-RAGE treated with CHX (0.25 mM) and HU (2 mM for 4 h). The samples were collected at the indicated time points. (**C**) Representative immunoblots showing the levels of Mcm2 in HeLa RAGE$^{-/-}$ cells expressing GFP-Mcm2 in combination with mCherry alone or the mCherry-RAGE treated with CHX (0.25 mM) and HU (2 mM for 4 h) and the samples were collected at the indicated time points.

fects on Mcm2 (Figure 5B; lanes 2–5). However, when the cells were expressing mCherry-RAGE, a persistent stable level of Mcm2 (Figure 5B) was observed. More importantly, this was evident from the shortest time point (1 h) to the latest timepoint (6 h) (Figure 5B; lanes 7–10). These data show that the RAGE/Mcm2 interaction stabilizes Mcm2.

To further confirm that the observed phenotype was not associated with poor expression of the endogenous Mcm2 and was indeed associated with the Mcm2 stability imparted by the presence of RAGE, GFP-tagged Mcm2 was expressed in conjunction with mCherry alone or with mCherry-tagged RAGE in Hela RAGE$^{-/-}$ cells. Like the observation made with endogenous Mcm2, nuclear RAGE promotes stability to Mcm2 under replication stress, as marked by the sustained levels of GFP-tagged Mcm2 during all time points studied (Figure 5C; lanes 8–10). However, in the cells expressing mCherry alone, Mcm2 was degraded over time (Figure 5C; lanes 3–5). Altogether, these data confirm that the RAGE stabilizes the Mcm2 levels in replication stress situations.

RAGE maintains the integrity of the nucleus

Replication stress prominently affects the organs showing a high turnover, such as the ciliated zones of the kidney, gut and endothelium (39). Therefore, RAGE$^{-/-}$ mice kidneys were studied along with age-matched background controls. Histological analysis of the RAGE$^{-/-}$ kidneys showed an elevated frequency of enlarged nuclei with an apparent disorganization of the nuclear morphology, known as karyomegaly (Supplementary Figure 13A, B; $P < 0.0001$; $n = 5$). In addition, renal cells from RAGE$^{-/-}$ mice had a higher frequency of micronuclei than the age-matched controls (Supplementary Figure 13C), as also observed in the cell lines tested. Both karyomegaly and micronuclei are associated with premature aging (40,41) and an abnormally high proliferation rate (42). Further, histological analysis of RAGE$^{-/-}$ kidneys showed a higher frequency of Ki67-positive cells than controls (Supplementary Figure 13D; $P < 0.0001$; $n = 5$).

In diabetes, a metabolic perturbation leads to the accumulation of dicarbonyls such as formaldehyde, glyoxal and

Table 2. Basic parameters of the patient cohort

Parameters	Controls	Diabetes	*P*-value
Number	n = 5	n = 5	
Age (years)	66.0 ± 3.1	73.2 ± 8.7	n.s.
Gender (f/m)	0/5	1/4	
BMI (kg/m^2)	27.6 ± 2.9	32.4 ± 10.1	n.s
Diabetes duration (years)	—	18.4 ± 12.7	<0.05
CVD (yes, *n* [%])	1 [20]	2 [40]	n.s.
Neuropathy (yes, *n* [%])	0 [-]	3 [60]	<0.05
Retinopathy (yes, *n* [%])	0 [-]	2 [40]	n.s.
Nephropathy (yes, *n* [%])	0 [-]	5 [100]	
Fasting glucose (mg/dl)	99.4 ± 9.1	205.6 ± 86.5	<0.05
HbA1c (%)	5.7 ± 0.3	8.8 ± 1.8	<0.01
Triglyceride (mg/dl)	87.8 ± 37.2	164.2 ± 50.3	<0.05
Cholesterol (mg/dl)	195.0 ± 54.2	164.8 ± 59.9	n.s
eGFR (ml/min*1.73m^2)	95.6 ± 4.0	37.2 ± 13.9	<0.0001
urinary ACR (mg/g)*	11.2 ± 8.5	880.8 ± 959.9	<0.05
Kreatinine	0.8 ± 0.1	1.9 ± 0.9	<0.05

Table 3. The number of mice surviving at the indicated treatment and duration

Background		WT		RAGE$^{-/-}$	
	Animal numbers (↓)	Control	STZ	Control	STZ
C57BL6					
	at the beginning	10	10	10	20
	at the end of 4 weeks	10	10	10	16
	at the end of 8 weeks	10	10	9	9
	at the end of 12 weeks	10	9	9	2
SV129					
	at the beginning	10	10	10	30
	at the end of 4 weeks	10	10	10	24
	at the end of 8 weeks	10	10	9	16
	at the end of 12 weeks	10	10	8	5

methylglyoxal (20,43–47). These reactive dicarbonyls react with nuclear proteins rich in basic amino acids (48). This might be involved in developing diabetic complications (49,50). When the frequency of micronuclei in non-smoking age-matched mononuclear cells isolated from controls or type-2 diabetic patients was studied, micronuclei formation was more prevalent in diabetic patients than controls (Supplementary Figure 14A, B; $P < 0.0001$; $n = 5$). Patients with type 2 diabetes and increased frequency of micronuclei were characterized by albuminuria and other organ complications (Table 2).

However, the increased frequency of micronuclei in pathological samples might be linked to multiple nuclear disturbances. To understand the contribution of the RAGE/Mcm2 axis in this increased frequency of micronuclei in diabetic PBMCs, RAGE/Mcm2 colocalization was studied in these cells. In PBMCs of patients with type 2 diabetes and nephropathy presenting with micronuclei, ∼58% showed a loss of RAGE/Mcm2 co-localization in the nucleus (Supplementary Figure 14C; $P < 0.0001$; $n = 5$). In contrast, this was not observed in the non-micronucleated PBMC from the same patients. Loss of RAGE/Mcm2 co-localization is consistent with the *in vitro* data, showing that the RAGE–Mcm interaction is essential for resolving replication stress. Thus, the RAGE/Mcm2 axis is important in replication stress that emerges from metabolic disease and might play an undiscovered role in developing diabetic complications.

If the RAGE/Mcm axis was essential, then the combination of metabolic stress, such as diabetes, with a RAGE$^{-/-}$ should result in increased toxicity. When age-matched control or RAGE$^{-/-}$ mice were injected with streptozotocin (STZ) to induce hyperglycemia, a very high mortality rate was observed in RAGE$^{-/-}$ mice (∼85–90% within 8 weeks of diabetes; Table 3). Thus, studies looking at the time course of renal complications were not possible in STZ-treated RAGE$^{-/-}$ mice. Therefore, background controls were studied after 3 months and RAGE$^{-/-}$ kidneys were studied only 7 weeks after diabetes induction. At 3 months, WT control kidneys showed prominent zones of ciliated acetylated-tubulin-positive cells in the glomerulus, which were not markedly reduced by STZ-induced hyperglycemia (Figure 6A, B). However, when hyperglycemia was induced in RAGE$^{-/-}$ mice, a substantial reduction of the acetylated-tubulin positivity was observed compared to the WT controls (Figure 6A, B; $P < 0.01$ to 0.001; $n = 5$). This is compatible with ciliopathy as a marker of replication stress.

A consequence of impaired DNA repair in diabetes is an increased accumulation of ECM, finally leading to loss of organ function (13). In RAGE$^{-/-}$ mice, Masson's Trichrome positivity, indicative of interstitial renal fibrosis, was evident in the kidneys of non-diabetic RAGE$^{-/-}$ mice, which was severely aggravated after STZ treatment (Figure 6C, D; $P < 0.0001$; $n = 5$). In addition to fibrosis, RAGE$^{-/-}$ kidneys also showed an increased number of cells with karyomegaly (Figure 6C, zoomed area). Thus, the absence of timely resolution of the endogenous replication stress and compromised repair in the STZ-treated RAGE$^{-/-}$ model system is associated with the onset and progression of interstitial fibrosis. Taken together, these data validate the importance of RAGE, whose absence results in a more severe STZ-induced phenotype, including lethality.

Furthermore, in addition to diabetes, metabolic abnormalities in cancer cells are known to be linked with glycolytic flux; therefore, cancer cells are also exposed to a situation similar to the metabolic disorder in diabetic PBMC (Garaycoechea, Crossan *et al.* 2018). Therefore, the presence of micronuclei was determined in SCLC. Human SCLC biopsies also show an increased frequency of micronuclei (Supplementary Figure 15), indicating that metabolic perturbations affecting the expression of micronuclei, are cumulatively operative in SCLC.

Replication stress is common in highly proliferating cancer cells and the ciliated zones of the diabetic kidney. In both of these situations, we observed an elevated frequency of micronuclei. Further, an increased expression of RAGE and Mcm2 was earlier reported in relapsed SCLC cases (14,51); therefore, immunolocalization of RAGE and Mcm2 was studied. Immunofluorescence analysis of RAGE and Mcm2 in the human SCLC tissue showed that micronucleated cells have a disturbed RAGE and Mcm2 localization, similar to the observation in PBMC from patients with type 2 diabetes and diabetic nephropathy. In contrast, the neighbouring cells did not lead to any visible micronuclei and had a prominent nuclear RAGE–Mcm2 localization (Supplementary Figure 16A). In micronucleated SCLC cells, four

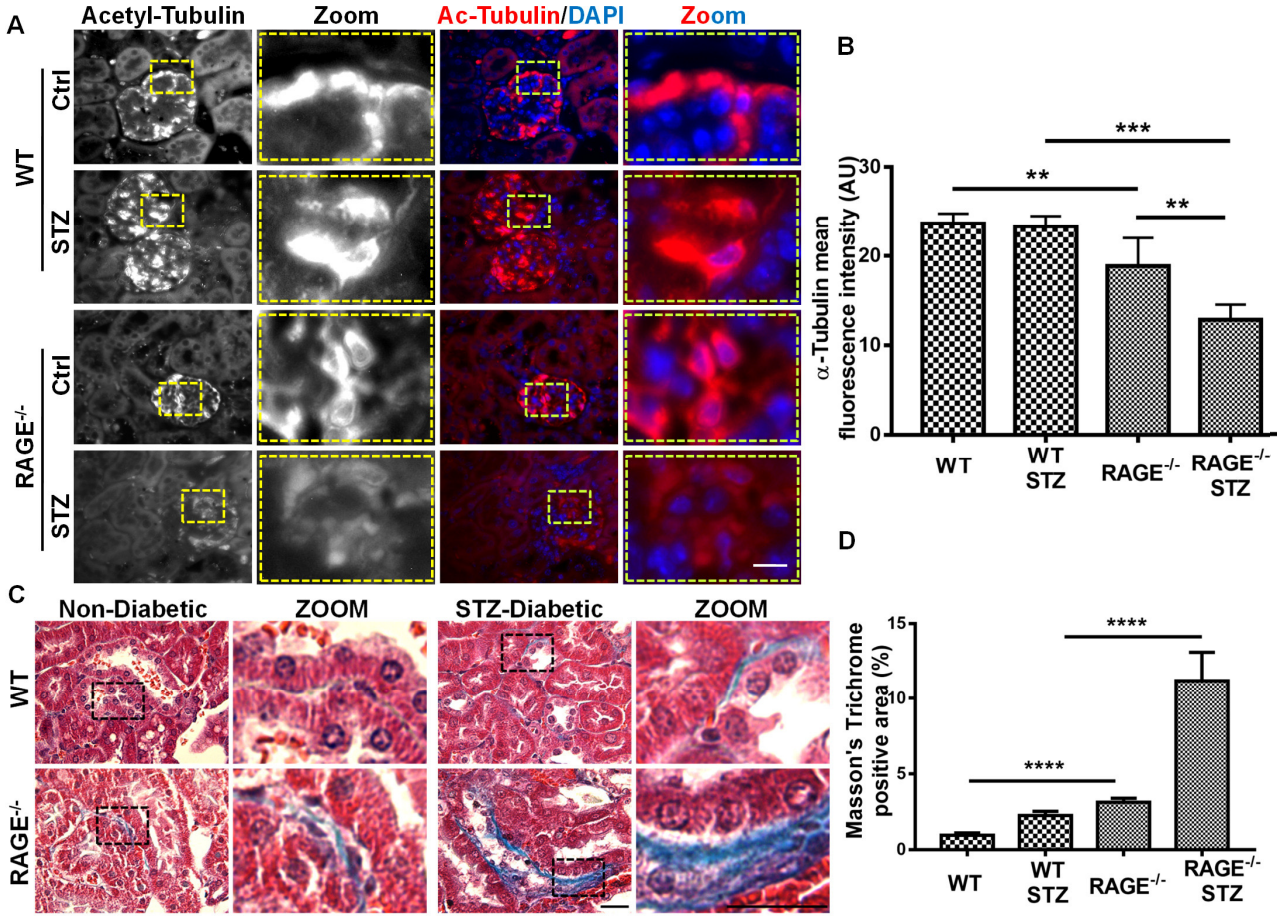

Figure 6. Absence of RAGE affects the integrity of ciliated zones and modulates the buildup of ECM. (**A**) Representative images of renal sections obtained age-matched controls versus non-diabetic (3 months old) or 7-week diabetic (STZ) WT and RAGE$^{-/-}$ mice, stained for ciliated zone marker α-acetylated-tubulin (in red). The areas marked in dotted boxes are shown in zoomed window (scale 50μm). DAPI (in blue) represents the nucleus. (**B**) Quantitative analysis representing the mean fluorescence intensity of α-acetylated tubulin in WT or RAGE$^{-/-}$ non-diabetic (–) or diabetic (+) renal section data presented in (A). Data represent mean ± SD, $^{**}P < 0.01$; $^{***}P < 0.001$, $n = 5$. (**C**) Representative images of renal sections from age-matched controls *vs* non-diabetic (3 months) or 7-week diabetic (STZ) WT and RAGE$^{-/-}$ mice showing the accumulation of ECM components, as stained by Masson's Trichrome, the ECM areas are recognized by its bluish staining (scale 50 μm). (**D**) Quantitative analysis representing the mean area showing accumulation of ECM components in renal sections of non-diabetic or diabetic WT or RAGE$^{-/-}$ mice. Data derived from (C). Data represent mean ± SD, $^{****}P < 0.0001$; $n = 5$.

different patterns of RAGE–Mcm2 staining were observed: (i) lack of RAGE and Mcm2 in the nucleus; [pointed with yellow arrow], (ii) absence of RAGE [pointed with blue arrow], (iii) lack of formation of foci containing RAGE and Mcm2 [pointed with orange arrow], (iv) aggregated RAGE [pointed with magenta arrow], (Supplementary Figure 16A). These findings were only present in micronucleated cells but not the normal neighbouring cells without any visible micronuclei. In these cells free of micronuclei, a prominent colocalization of RAGE–Mcm2 in the nucleus was evident (as shown in Supplementary figure 6). The RAGE/Mcm2 localization was studied in the total micronucleated cells of the SCLC biopsies. It was observed that about 61% of the micronucleated cells from SCLC showed an aberrant localization pattern for RAGE or Mcm2 (Supplementary Figure 16B; $P < 0.01$–0.0001; $n = 5$). These correlative observations are consistent with the *in vitro* data, thus suggesting a critical function of the RAGE–Mcm2 axis during replication stress.

Similar to PBMC or SCLC samples, a disturbed pattern for the RAGE–Mcm2 axis was also evident in murine (Supplementary Figure 17; $n = 3$) and human kidney sections derived from STZ-induced experimental diabetes or the type-2 diabetic patients diagnosed with interstitial fibrosis (Supplementary Figure 18; $n = 3$), respectively. About 72% of the micronucleated cells in STZ kidneys showed a disturbed localization pattern for RAGE or Mcm2 (Supplementary Figure 19A; $P < 0.0001$; $n = 3$), whereas about 57% of the micronucleated cells in human kidneys with interstitial fibrosis showed this feature (Supplementary Figure 19B; $n = 3$). This shows that the nuclear disturbances marked by micronuclei in the cells derived from these pathological situations showed a comparable perturbed localization pattern.

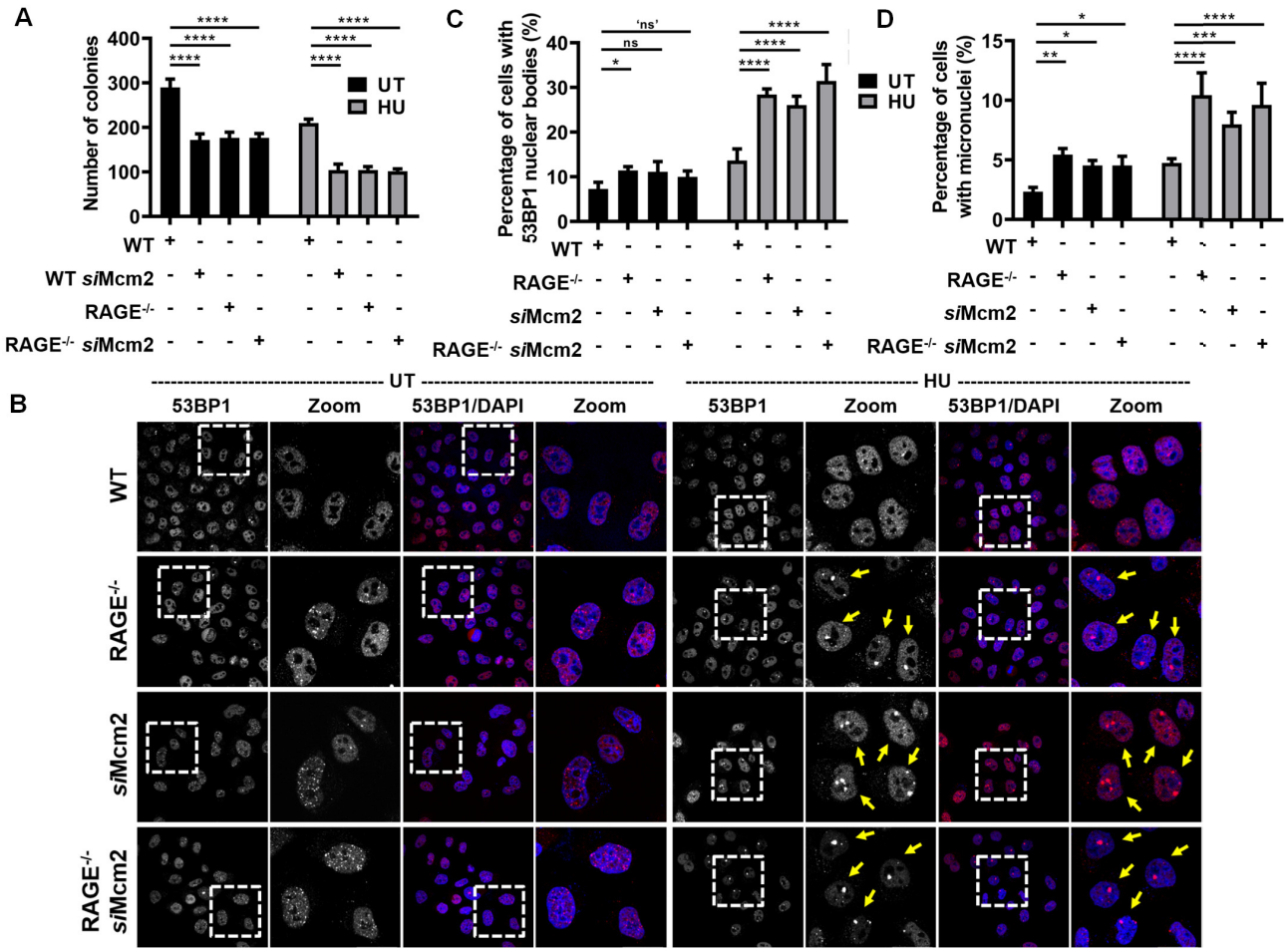

Figure 7. RAGE and Mcm2 participate in the same pathway to counter the replication stress. (**A**) Quantitative analysis showing the percentage survival potential of untreated (UT; black bars) and hydroxyurea treated (HU; 2 mM, 4 h; grey bars), Mcm2 depleted WT or RAGE$^{-/-}$ HeLa cells as described in Supplementary Figure 20B. Data represent mean ± SD, ****$P < 0.0001$; $n = 6$. (**B**) Representative images showing the pattern of 53BP1 (in red) stained after 16 h of post-recovery of HU (2 mM, 4 h) treated and Mcm2 depleted WT or RAGE$^{-/-}$ Hela cells. DAPI (in blue) represents the nucleus, and the zoom window (in dotted white boxes) represents the respective 3x zoomed areas (scale 25 μm). (**C**) Quantitative analysis showing the mean percentage of 53BP1 marked OPT domains from the cells described in (B). Data represent mean ± SD, *$P < 0.05$, ****$P < 0.0001$, ns represents non-significant; $n = 3$. In this figure, ns represents the comparison between single depletion/deletion, whereas 'ns' indicates double depletion/deletion. (**D**) The quantitative analysis showing the frequency of micronuclei from HU-treated cells. Data represent mean ± SD, *$P < 0.05$, **$P < 0.01$; ***$P < 0.001$; ****$P < 0.0001$; $n = 3$.

RAGE and Mcm2 participate in the same pathway to counter replication stress

Timely resolution of the replication defects involves multiple pathways involving various nucleases and helicases. We next studied whether RAGE and Mcm2 respond to replication stress by using the same routes. Therefore markers of post-replication stress, such as 53BP1 and the frequency of micronuclei, were studied in RAGE$^{-/-}$ cells that were either mock-transfected or depleted of their endogenous Mcm2 (siMcm2) (Supplementary Figure 20A). Both the absence of RAGE or depletion of Mcm2 resulted in a significant decrease in survival potential compared to untreated counterparts of these cells under replication stress situation (Figure 7A, Supplementary Figure 20B; $P < 0.0001$; $n = 6$). The depletion of Mcm2 from RAGE$^{-/-}$ did not alter their HU sensitivity. Furthermore, neither the absence of RAGE nor the depletion of Mcm2 could enhance the frequency of 53BP1 marked OPT domains in these cells (Figure 7B and C; $P < 0.05$–0.0001; $n = 3$), consistent with the data on survival potential. Further evaluation of the effect of Mcm2 depletion on the frequency of micronuclei in WT and RAGE$^{-/-}$cells revealed that the single or combined deficiency of Mcm2 and RAGE did not add-on the effects of an already missing factor (Figure 7D, Supplementary Figure 20C; $P < 0.05$–0.0001; $n = 3$). Furthermore, induction of replication stress by glyoxal also showed a similar phenotype in the colony-forming assay (Supplementary Figure 21A, B; $P < 0.0001$; $n = 6$), micronuclei frequency (Supplementary Figure 21C, D; $P < 0.05$–0.01; $n = 6$), and the 53BP1 expression in OPT domain (Supplementary Figure 22A, B; $P < 0.05$–0.0001; $n = 6$).

These data are consistent with the hypothesis that RAGE and Mcm2 respond to replication stress *via* the same pathway. Removal of one or another player of this corresponding pathway compromises this response; that might explain

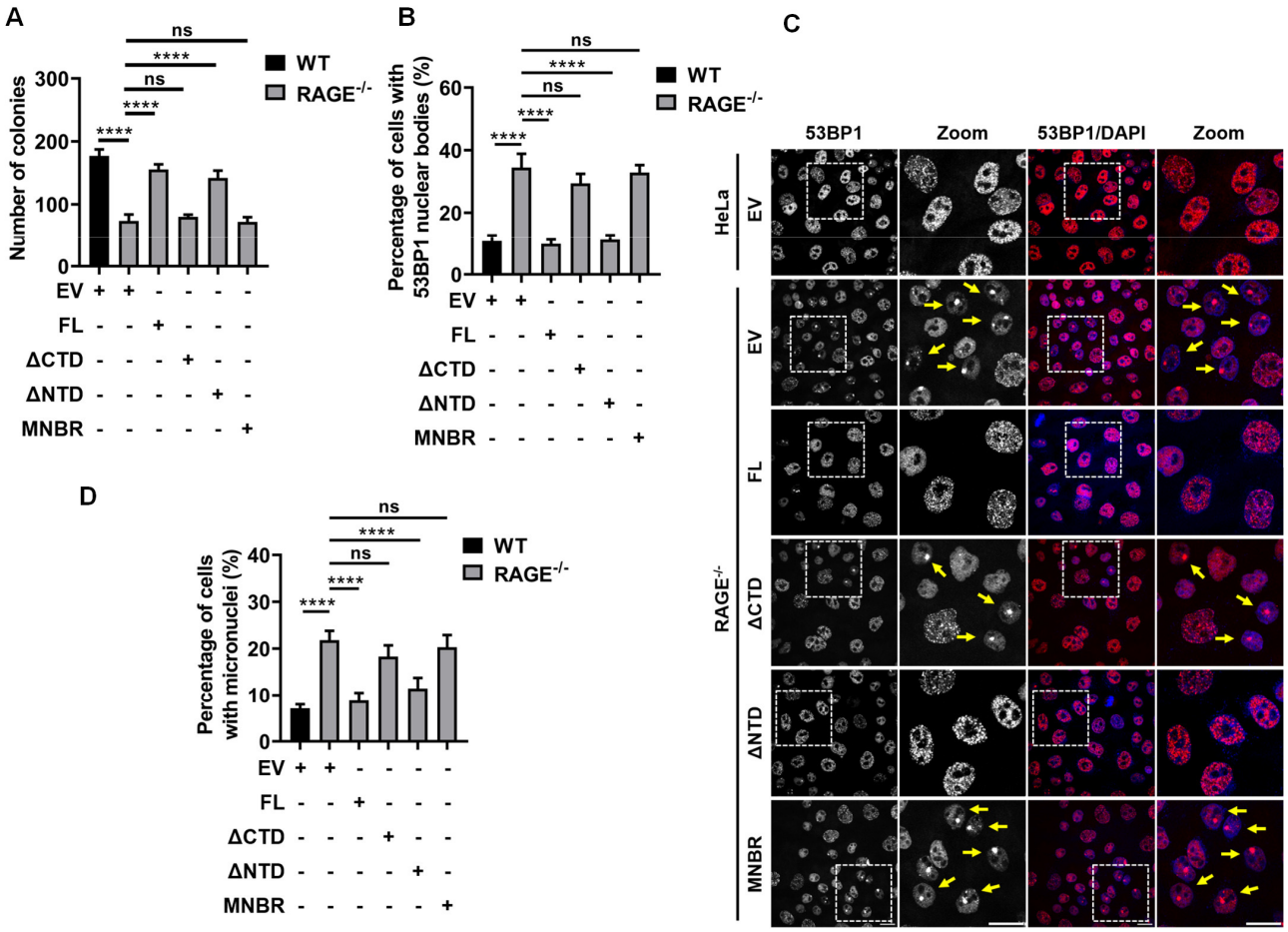

Figure 8. Reconstitution of RAGE promotes the remission of replication stress-associated defects. (**A**) The graphical presentation of the total number of colonies formed from the assay is shown in Supplementary Figure 24 A. Data represent mean ± SD, ****$P < 0.0001$; $n = 6$. Panel EV represents the cells transfected with an empty vector, FL represents full-length RAGE, ΔCTD or ΔNTD represents the deletion constructs, and MNBR represents Mcm2 non-binding RAGE. Details of these constructs were described in Supplementary Figure 2 A. (**B**) The graphical presentation of the total number of OPT domain associated large 53BP1 foci is shown in Figure 8C. Data represent mean ± SD, ****$P < 0.0001$; $n = 3$; >300 cells were analyzed for each condition. (**C**) Representative images of the OPT domain associated single large 53BP1 foci observed in HU (2 mM, 4 h) treated WT or RAGE$^{-/-}$ Hela cells reconstituted with the various RAGE constructs. The areas marked in dotted boxes are shown in the zoomed window. The abbreviations for EV, FL, ΔNTD, ΔCTD, and MNBR are mentioned in (A) (scale 25 μm). (**D**) Quantitative analysis of the frequency of micronuclei in WT and RAGE$^{-/-}$ HeLa cells shown in Supplementary Figure 25. Data represent mean ± SD, ****$P < 0.0001$; $n = 3$; >240 cells were analyzed for each condition.

why an additional removal or depletion does not sensitize these cells further to the replication stress-inducing agents.

Reconstitution of RAGE resolves replication stress and improves survival in RAGE$^{-/-}$ cells

Replication stress and its associated signaling perturb the normal cellular homeostasis of RAGE$^{-/-}$ cells. RAGE$^{-/-}$ cells were reconstituted with full-length, MNBR, N- or C-terminal deletion mutants of RAGE (see Supplementary Figure 2A). The cells reconstituted with full-length nuclear RAGE showed better survival potential when compared to empty vector or MNBR-complemented cells (Figure 8A, Supplementary Figures 23, 24A). The C-terminal deleted RAGE construct did not improve the survival potential of cells, while the N-terminal deleted RAGE, missing amino acids 1–140, was as effective as full-length RAGE (Figure 8A, and Supplementary Figure 24A; $P < 0.001$; $n = 6$). Consistent with the functional effect, the N-terminal deleted RAGE maintains maximal binding to Mcm2 (see Figure 1F) when immunoprecipitation was performed from HU-treated cells. This might be because the N-terminus deletion potentially unmasks the regulatory DNA binding region of RAGE and thus might generate a better affinity for DNA binding.

To validate the importance of full-length, MNBR or ΔNTD RAGE reconstitution under basal and replication stress situations, glyoxal was used. Similar to the observations made with HU, full-length, but not MNBR or EV, could functionally complement Hela RAGE$^{-/-}$ cells against glyoxal-induced replication stress (Supplementary Figure 24B, C; $P < 0.0001$; $n = 6$). Furthermore, the full-length and the N-terminal deleted RAGE construct did normalize the cell survival under HU-induced replication stress and prevented the formation of single large 53BP1 foci in OPT domain (Figure 8B, C; $P < 0.0001$; $n = 3$) and micronuclei formation (Figure 8D, and Supplementary Figure 25; $P < 0.0001$; $n = 3$). In contrast, as expected, MNBR

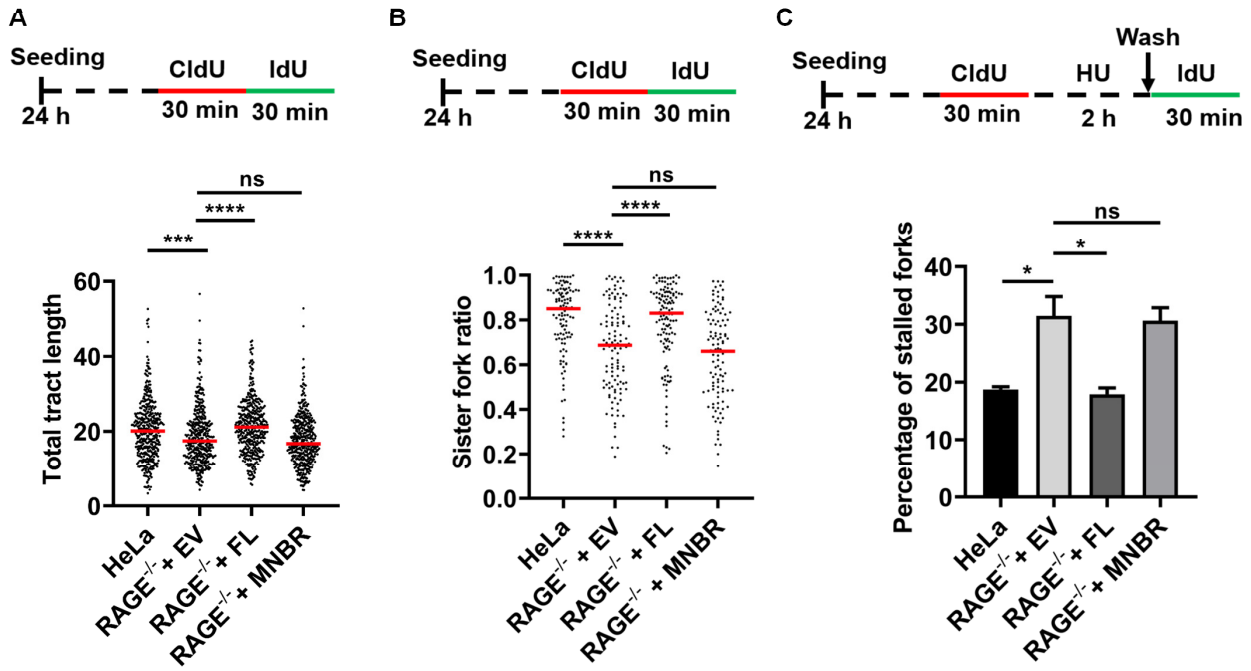

Figure 9. Restoration of RAGE levels promotes the increased tolerance to replication stress. (**A**) Schematic preview and the quantitative data showing the length of tracts observed in DNA fiber assay in Hela RAGE$^{-/-}$ cells complemented with full-length, MNBR or the EV. The Hela (Hela RAGE$^{+/+}$) cells served as an internal control. The red bar indicates median. Mann-Whitney non-parametric test was used to compare the differences. For quantification >200 tracts were scored for each data set; ***$P < 0.001$; ****$P < 0.0001$; $n = 3$. (**B**) Schematic preview and quantitative fiber spreading data, showing the ratio of sister forks. Hela RAGE$^{-/-}$ cells complemented with either full-length, MNBR or the EV. The Hela (Hela RAGE$^{+/+}$) cells served as an internal control. The red bar indicates median. Mann-Whitney non-parametric test was used to compare the differences. For quantification >40 tracts were scored for each data set; ****$P < 0.0001$; $n = 3$. (**C**) Quantitative fiber spreading data showing the percentage of stalled (CldU only) forks from HeLa RAGE$^{-/-}$ cells complemented with full-length, MNBR or the EV. The Hela (Hela RAGE$^{+/+}$) cells served as an internal control. For quantification >200 tracts were scored for each data set; *$P < 0.05$; $n = 4$.

or EV imparted no benefits to the RAGE$^{-/-}$ cells (Figure 8D, and Supplementary Figure 25). When glyoxal was used as a replication stress-inducing agent, similar results 53BP1 (Supplementary Figure 26A, B; $P < 0.0001$; $n = 6$) and micronuclei frequency were obtained (Supplementary Figure 27A, B; $P < 0.0001$; $n = 6$).

To reverify if the absence of RAGE-associated replication stress defects could be reverted in another model system, RAGE$^{-/-}$ lung fibroblasts were complemented with either full-length nuclear RAGE, the empty vector alone (EV) or the MNBR, which served as a negative control. Similar to the observations made with Hela cells, the complementation of RAGE$^{-/-}$ lung fibroblasts with full-length RAGE, but not with MNBR or EV normalized the timely recovery from the replication stress as marked by the 53BP1 large foci (Supplementary Figure 28A, B; $P < 0.0001$; $n = 6$), micronuclei frequency (Supplementary Figure 29A, B; $P < 0.0001$; $n = 6$), and survival potential (Supplementary Figure 30; $P < 0.0001$; $n = 6$) after HU-induced replication stress. Like HU, glyoxal-induced replication also confirmed these observations (Supplementary Figure 31A, B and C; $P < 0.0001$; $n = 6$). Collectively, these molecular reconstitution experiments clarified the defects associated with the absence of RAGE, or impaired RAGE–Mcm2 axis, particularly under replication stress.

To verify if the increased survival, decreased micronuclei and 53BP1 nuclear bodies in Hela RAGE$^{-/-}$ cells complemented with full-length RAGE, but not MNBR or EV, indeed associated with decreased replication defects, DNA fibre assay was performed with these complemented groups of Hela RAGE$^{-/-}$ cells. Hela RAGE$^{+/+}$ served as a positive control of the experiment. It was observed that complementation of Hela RAGE$^{-/-}$ cells with full-length RAGE, but not with MNBR or mCherry alone could rescue the replication fork slowing and sister fork asymmetry phenotypes of these cells (Figure 9A, B; $P < 0.001$ to 0.0001; $n = 3$). The expression of these complementation constructs was verified using a fluorescence intensity score (Supplementary Figure 32). In addition, the replication fork stalling following HU treatment was dramatically reduced in Hela RAGE$^{-/-}$ cells complemented with full-length nuclear RAGE (Figure 9C; $P < 0.05$; $n = 4$). However, neither mCherry alone nor the MNBR could suppress the fork-stalling phenotype of the Hela RAGE$^{-/-}$ cells (Figure 9C). These data suggest that the improved survival, decreased 53BP1 foci, and the micronuclei frequency in Hela RAGE$^{-/-}$ cells complemented with full-length RAGE were indeed associated with the improved potential of these cells against replication stress.

Most of the high proliferating cells, including Hela, are known to harbour chemo- and mechanosensory cilia on their cell surface (52). Our data show that the compromised replication stress response is indeed associated with ciliopathy, as marked by the loss of ciliated zones around

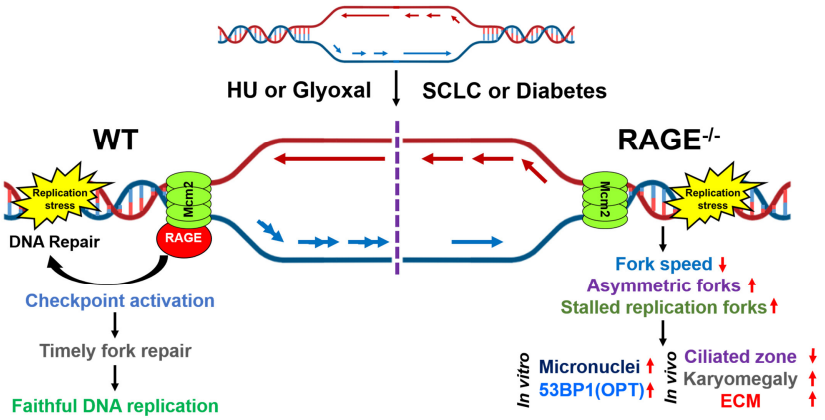

Figure 10. Role of RAGE in faithful progression of the replication fork and its stability under basal conditions or replication stress. The scheme shows the cellular response to the replication stress in the presence or absence of RAGE. The perturbed homeostasis and failure to resolve the replication errors may play a role in various diseases, such as cancer and diabetic complications.

the tubular cells. To validate that the pathological implications observed in the RAGE$^{-/-}$ kidney were linked to the RAGE/Mcm2 axis, RAGE complementation in RAGE$^{-/-}$ Hela was further explored. The RAGE$^{-/-}$ cells were complemented with either full-length RAGE, MNBR or the vector expressing mCherry alone and were either left untreated or treated with the replication stress agent HU (2 mM for 4 h). After 5 days of the replication stress, the status of cilia-associated acetylated tubulin was determined. It was observed that full-length nuclear RAGE in basal or replication stress increased the level of acetylated tubulin (Supplementary Figure 33, lane 3 or 7). In contrast, neither the Mcm2 non-binding RAGE (MNBR) nor the empty vector (EV) promoted ciliogenesis in basal or replication stress (Supplementary Figure 33). This supports the notion of an important role of the RAGE/Mcm2 axis in the coordinated synchrony of proliferating cells.

DISCUSSION

This study provides a partial answer to the open question of how the Mcm complex is recruited during replication stress and its sustained activity. We find that both, Mcm2 and 7 bind RAGE *via* the far N- and the C-terminal region of RAGE, while the N-terminal region of RAGE binds DNA at the site of damage. Depleting these 2 components results in enhanced sensitivity to replications stress. The nuclear RAGE/Mcm axis plays a vital role in the faithful progression of the replication fork under stress situations, particularly by ensuring synchrony of bidirectional fork progression to maintain a normal sister fork ratio, thus preventing fork stalling (Figure 10). Our data indicate that lack of RAGE affects the timely resolution of the replication defects *in vitro* and *in vivo* models.

RAGE$^{-/-}$ cells show a very high frequency of micronuclei, the expression of 53BP1 in OPT (Oct1-PTF-Transcription) domains in the nucleus is associated with reduced survival of these cells under replication stress situation (37). A similar observation was previously reported for cells depleted of Mcm2, 53BP1 or Mus81, known to participate in the maintenance of the replication fork (37,38,53–57). Moreover, at the level of DNA replication, RAGE$^{-/-}$ cells showed not only an increased frequency of stalled replication forks but also a slowed rate of DNA synthesis, indicating a perturbed DNA replication process, despite the presence of and intact CHK1 S345 signaling in HU-treated RAGE$^{-/-}$ and WT (RAGE$^{+/+}$) Hela cells. Depletion of either RAGE or Mcm2 and reconstitution of the pathways indicated that both act together in the same pathway.

From the differences in the staining patterns of RAGE and Mcm2 in cancer and non-malignant renal tissue under replications stress, one might speculate that (i) different signals are responsible for the different morphological features indicating a non-functional RAGE/Mcm axis, (ii) that cells respond in a cell or organ-specific manner, or (iii) that the different staining patterns are the result of different stages of replication stress. Furthermore, the signals leading to the apparent loss of the RAGE/Mcm2 axis in cells expressing micronuclei remain unknown.

Furthermore, it remains to be shown how the RAGE/Mcm axis protects the cell from replications stress. Several models might explain how the RAGE/Mcm axis provides an optimal template for handling replication stress. One is that RAGE supports Mcm binding to the site of DNA damage due to the ability of RAGE to bind DNA with the N-terminal region and Mcm with the C-terminal region. A second option is that Mcm2 bound to RAGE is protected from non-enzymatic protein modification or inactivation by ROS, as previous data have shown that RAGE is relatively resistant to modification by oxidative stress (unpublished results). In addition, it remains unknown whether any of the kinases initiating the repair cascade are involved in the posttranslational modifications of RAGE (12,13). Future studies have to resolve these issues, while the ATM/ATR and checkpoint signaling cascade activate RAGE by phosphorylating its Serine(s) to initiate and execute the repair process (58), the data presented show that RAGE does not directly contribute to the initial replication stress signaling (Figure 4A, B; and Supplementary Figure 9B). Thus the RAGE/Mcm

axis is operative further downstream in ensuring the faithful progression of the replication fork under stress situations.

The progression of replication forks (44,45,59–62) is impaired in many diseases, including cancer, metabolic diseases, diseases resulting in the formation of fibrosis and others. However, it is beyond the scope of this manuscript to extend the observations made in this study to all these different pathologic states associated with replications stress, formation of micronuclei, karyomegaly, and fibrosis. However, in support of such a broad relevance of the model presented and previous data showing that nuclear RAGE is present in all cells after irradiation (12) and that therapeutic application of a phosphomimetic RAGE mutant can initiate the resolution of renal and pulmonary fibrosis in 2 models of experimental diabetes (12,13,46,47). In addition, fibrosis is observed in several pathologic states associated with a sterile form of inflammation. Previously, we have shown that nuclear RAGE can reverse not only this metabolic stress-induced fibrosis (13) but also attenuates the inflammatory cascade initiated by DNA damage, senescence and the senescence-associated secretory phenotype (SASP) (12,13,63). For understanding the fibrosis cascade, which in cancer and diabetes is at the early stages focal, it might be important that the micronuclear DNA can be either incorporated into the genome *via* DNA repair initiated in the next cell cycle (64,65) or undergoes non-specific lethal rearrangement or pulverization (19,66). It remains unknown whether, in the absence of a functional RAGE/Mcm2 axis, micronuclei execute a sterile inflammatory cascade (67), participating in addition to the DNA damage response to inflammation and fibrosis. In micronucleated cells, some, but not all, show an impaired nuclear localization of RAGE (12,33) and a lack of nuclear Mcm. It remains unknown whether the nuclear translocation of RAGE and Mcm is impaired in replication stress or whether nuclear RAGE and Mcm are exported or degraded, potentially due to an enzymatic or non-enzymatic modification under stress conditions.

The Mcm complex comprises seven subunits that timely assemble on the replication origin to form the pre-replication complex in a Dbf4-dependent kinase Cdc7 (DDK) manner (53). In our study, we have observed that upon replication stress, RAGE interacts with Mcm2 and Mcm7. However, the functional role of other subunits of the Mcm complex and the DDK remains to be explored. The Mcm subunit binding RAGE might differ in different states of replication stress and between the different cell types involved.

As a pattern recognition factor belonging to the immunoglobulin family, RAGE can be expressed in the membrane, the mitochondria and the nucleus and bind various proteins. These include proteins playing a direct role in DNA repair and replication fork integrity, such as MRE11, HMGB1, members of the S100 family and others (68–72). Future studies are needed on how these proteins affect the RAGE/Mcm axis. Therefore, it is plausible that MRE11 or Mcm2 might be competing for binding to RAGE. At the cell surface, RAGE is also known to induce a sustained pro-inflammatory cellular response (71,73–78). This raises the question of how other RAGE ligands, binding extracellular membrane-localized RAGE domains (74,77,78) or nuclear factors such as Mus81, Fen1, FANCD2, Par3 and Ku70/80 heterodimers, involved in maintaining genomic stability (79,80) (81), interact with the RAGE/Mcm cascade described here.

At the physiological level, replication stress prominently affects the organs showing higher cellular turnover, such as bone marrow, kidney tubules, gut and endothelium (5). More importantly, $ATR^{-/-}$ mice showed multiple organ failure, increased organ fibrosis, carcinoma formation, and premature embryonic death (82,83). In addition, the loss of Mus81 nuclease, which is involved in processing the entangled chromosomes, also showed karyomegaly and interstitial nephritis (84). Similarly, CEP290 loss is associated with persistent DNA damage signaling and a broad range of ciliopathies (85). More importantly, the accumulation of endogenous DNA damage in $RAGE^{-/-}$ cells is attributed to compromised DNA repair and disturbed replication forks. It is important to note that depletion of NEK8, CEP290 showed similar sensitivity to replication stress, decreased fork velocity, abnormal fork symmetry and increased fork stalling (7,85), as observed in the $RAGE^{-/-}$ model system.

Previous studies in the kidney have shown that karyomegalic nephritis and ciliopathies are associated with

Table 4. Details of primary and secondary antibodies

Antibody	Brand/source	Catalog
Mcm2	Cell Signaling Technology	Cat#4007S
Mcm7	Cell Signaling Technology	Cat#3735S
mCherry	ChromoTek	Cat#5f8-100
GFP	ChromoTek	Cat#PABG1-100
CHK1	Cell Signaling Technology	Cat#2360S
pCHK1-S345	Cell Signaling Technology	Cat#2348S
RAGE	R&D Systems	Cat#MAB1179
RAGE	R&D Systems	Cat#MAB11451
RAGE	Helmholtz Zentrum Munich	Cat#9B6-1-1
Cyclin-A	Santa Cruz Biotechnology	Cat#sc-271682
53BP1	Novus Biologicals	Cat#NB100-304
53BP1	Bethyl Laboratories	Cat#A700-011
Histone H2A	Cell Signaling Technology	Cat#12349
GST Tag	Thermo Fisher Scientific	Cat#MA4-004
6x-His Tag	Thermo Fisher Scientific	Cat#MA1-21315
Actin	Cell Signaling Technology	Cat#8457S
PCNA	Cell Signaling Technology	Cat#13110S
RPA2	ABGENT	Cat#AP9115a
Tubulin	Thermo Fisher Scientific	Cat#14–4510-80
Acetylated-Tubulin	Sigma-Aldrich	Cat#T8203
Ki67	Thermo Fisher Scientific	Cat#14-5698-82
anti-BrdU antibody	Abcam	Cat#ab6326
anti-BrdU antibody	BD Biosciences	Cat#347580
Anti-rabbit IgG-HRP	Cell Signaling Technology	Cat#7074
Anti-mouse IgG-HRP	Cell Signaling Technology	Cat#7076
Anti-rat IgG-HRP	Cell Signaling Technology	Cat#7077
Anti-rabbit-Alexa-555	Abcam	Cat#Ab150074
Anti-rat-Alexa-647	Abcam	Cat#Ab150155
Anti-rabbit DyLight 488	Novus Biologicals	Cat#NBP1-75285
Anti-rat Cy3	Jackson Immuno Research	Cat#712-166-153
Anti-mouse Alexa 488	Thermo Fisher Scientific	Cat#A110334

Table 5. Information on cloning oligos

Silencer pre-designed siMcm2	Sense: CCAUCUAUCAGAACUACCAtt Antisense: UGGUAGUUCUGAUAGAUGGtc
RAGE ΔCTD	CCCTGCAGGGTAGTCGACCTCTGACACACATGT
RAGE ΔNTD	CTAATGAGAAGGGAAGATCTGTGAAGGAACAGACCAGG
RAGE MNBR C-del	GTCACATGTGTTGGGGGCTATCTTCTGCTTCC
RAGE MNBR K173A	AAGGGAGTATCTGTGGCTGAACAGACCAGGAGACAC
RAGE lacI	GTATAGGTACCATGCAAAACATCACAFCCCGGATTGGCGA and TATACCGCGGCTGCCCGCTTTCCAGTCGGGAAA
RAGE (murine and human)	(13,14) and (12)
Mcm2 (human)	ATAGAATTCTATGGCGGAATCATCGGAATCCTTCACCATGGCAT and ATATGGTACCGAACTGCTGCAGGATCATTTTCCTTTTCAGGTC

replication fork stalling, unscheduled origin firing and fork collapse (26,41). Similarly, the RAGE$^{-/-}$ kidney showed enlarged nuclei in the kidney tubules and decreased acetylated-tubulin signal in tubular and glomerulus zones across the RAGE$^{-/-}$ kidney. This situation was severely aggravated in diabetic RAGE$^{-/-}$ kidneys compared to age-matched non-diabetic and diabetic WT (RAGE$^{+/+}$) control kidneys. Further, the cyclin-dependent kinase inhibitors were shown to promote the regeneration of ciliated zones in the CEP290$^{-/-}$ model system (7,85). Likewise, the effect of these inhibitors in this inflammatory kidney complication in the RAGE$^{-/-}$ model system needs to be investigated.

In conclusion, our study establishes that the RAGE–Mcm2 axis is critical for a timely response against replication stress to prevent the replication forks from stalling. Further, metabolic or cellular interference of the RAGE–Mcm2 functional axis might contribute to the onset or the progression of replication stress-dependent diseases, such as diabetes and its complications and cancer.

DATA AVAILABILITY

The data underlying this article will be shared on reasonable request to the corresponding authors. In addition, data relating to this manuscript will be deposited at the medical faculty of the University of Heidelberg.

SUPPLEMENTARY DATA

Supplementary Data are available at NAR Online.

ACKNOWLEDGEMENTS

We thank all members of our group and the members of ALMF, Dr Stefan Terjung, Dr Beate Neumann, Ms Claudia Martin, Mr Vijay Thoutam of EMBL-Heidelberg for their support. The authors thank Prof Axel Roers for his kind support. The authors also thank Prof. Esther Herpel, Dr Nadine Volk and other members of the Institute of pathology (Heidelberg University) for tissue from patients with type-2 diabetes and nephropathy (Project number 2726).

Author contributions: V.K. P.J. and P.N conceptually designed the experiments; Z.H., M.A., B.M. and S.K., performed the experimental work. Z.K., S.K., A.S. and L.K. arranged the patient material used in this study. V.K., P.J. and P.N. wrote the manuscript.

FUNDING

Deutsche Forschungsgemeinschaft [SFB 1118 & GRK 1874-DIAMICOM]; Deutsches Zentrum für Diabetesforschung (DZD e.V. - Complications Academy); DZD [82DZD07C2G to A.S.]; Swiss National Science Foundation [310030_184716 to P.J.]; Czech Science Foundation [22-08294S to P.J.]. Funding for open access charge: Uniklinikum Heidelberg and SFB1118.

Conflict of interest statement. None declared.

REFERENCES

1. Gardner,A.F. and Kelman,Z. (2019) Editorial: the DNA replication machinery as therapeutic targets. *Front. Mol. Biosci.*, **6**, 35.
2. Hao,J. and Zhu,W. (2015) Maintain genomic stability: multitask of DNA replication proteins. *Transcr Open Access*, **3**.
3. Blow,J.J. (2019) Defects in the origin licensing checkpoint stresses cells exiting G0. *J. Cell Biol.*, **218**, 2080–2081.
4. Bleichert,F. (2019) Mechanisms of replication origin licensing: a structural perspective. *Curr. Opin. Struct. Biol.*, **59**, 195–204.
5. Zeman,M.K. and Cimprich,K.A. (2014) Causes and consequences of replication stress. *Nat. Cell Biol.*, **16**, 2–9.
6. Cimprich,K.A. and Cortez,D. (2008) ATR: an essential regulator of genome integrity. *Nat. Rev. Mol. Cell Biol.*, **9**, 616–627.
7. Choi,H.J., Lin,J.R., Vannier,J.B., Slaats,G.G., Kile,A.C., Paulsen,R.D., Manning,D.K., Beier,D.R., Giles,R.H., Boulton,S.J. *et al.* (2013) NEK8 links the ATR-regulated replication stress response and S phase CDK activity to renal ciliopathies. *Mol. Cell*, **51**, 423–439.
8. Cortez,D. (2015) Preventing replication fork collapse to maintain genome integrity. *DNA Repair (Amst.)*, **32**, 149–157.
9. D'Angiolella,V. and Guardavaccaro,D. (2017) Two paths to let the replisome go. *Cell Death Differ.*, **24**, 1140–1141.
10. Yoo,H.Y., Shevchenko,A., Shevchenko,A. and Dunphy,W.G. (2004) Mcm2 is a direct substrate of ATM and ATR during DNA damage and DNA replication checkpoint responses. *J. Biol. Chem.*, **279**, 53353–53364.
11. Bierhaus,A., Humpert,P.M., Morcos,M., Wendt,T., Chavakis,T., Arnold,B., Stern,D.M. and Nawroth,P.P. (2005) Understanding RAGE, the receptor for advanced glycation end products. *J. Mol. Med. (Berl.)*, **83**, 876–886.
12. Kumar,V., Fleming,T., Terjung,S., Gorzelanny,C., Gebhardt,C., Agrawal,R., Mall,M.A., Ranzinger,J., Zeier,M., Madhusudhan,T. *et al.* (2017) Homeostatic nuclear RAGE-ATM interaction is essential for efficient DNA repair. *Nucleic Acids Res.*, **45**, 10595–10613.
13. Kumar,V., Agrawal,R., Pandey,A., Kopf,S., Hoeffgen,M., Kaymak,S., Bandapalli,O.R., Gorbunova,V., Seluanov,A., Mall,M.A. *et al.* (2020) Compromised DNA repair is responsible for diabetes-associated fibrosis. *EMBO J.*, **39**, e103477.
14. Madhavan,B.K., Han,Z., Singh,B., Bordt,N., Kaymak,S., Bandapalli,O.R., Kihm,L., Shahzad,K., Isermann,B., Herzig,S. *et al.* (2021) Elevated expression of the RAGE variant-V in SCLC mitigates the effect of chemotherapeutic drugs. *Cancers (Basel)*, **13**, 2843.
15. Madhavan,B.K., Han,Z., Sickmann,A., Pepperkok,R., Nawroth,P.P. and Kumar,V. (2021) A laser-mediated photo-manipulative toolbox

for generation and real-time monitoring of DNA lesions. *STAR Protoc.*, **2**, 100700.
16. Soutoglou,E. and Misteli,T. (2008) Activation of the cellular DNA damage response in the absence of DNA lesions. *Science*, **320**, 1507–1510.
17. Han,Z., Madhavan,B.K., Kaymak,S., Nawroth,P. and Kumar,V. (2022) A fast and reliable method to generate pure, single cell-derived clones of mammalian cells. *Bio. Protoc.*, **12**, e4490.
18. Chevallet,M., Luche,S. and Rabilloud,T. (2006) Silver staining of proteins in polyacrylamide gels. *Nat. Protoc.*, **1**, 1852–1858.
19. Ying,S., Minocherhomji,S., Chan,K.L., Palmai-Pallag,T., Chu,W.K., Wass,T., Mankouri,H.W., Liu,Y. and Hickson,I.D. (2013) MUS81 promotes common fragile site expression. *Nat. Cell Biol.*, **15**, 1001–1007.
20. Deshpande,D., Agarwal,N., Fleming,T., Gaveriaux-Ruff,C., Klose,C.S.N., Tappe-Theodor,A., Kuner,R. and Nawroth,P. (2021) Loss of POMC-mediated antinociception contributes to painful diabetic neuropathy. *Nat. Commun.*, **12**, 426.
21. Chappidi,N., Nascakova,Z., Boleslavska,B., Zellweger,R., Isik,E., Andrs,M., Menon,S., Dobrovolna,J., Balbo Pogliano,C., Matos,J. *et al.* (2020) Fork cleavage-religation cycle and active transcription mediate replication restart after fork stalling at co-transcriptional R-loops. *Mol. Cell*, **77**, 528–541.
22. Kim,S.Y. and Hakoshima,T. (2019) GST pull-down assay to measure complex formations. *Methods Mol. Biol.*, **1893**, 273–280.
23. Kao,S.H., Wang,W.L., Chen,C.Y., Chang,Y.L., Wu,Y.Y., Wang,Y.T., Wang,S.P., Nesvizhskii,A.I., Chen,Y.J., Hong,T.M. *et al.* (2015) Analysis of protein stability by the cycloheximide chase assay. *Bio Protoc*, **5**, e1374.
24. Hofmann,M.A., Schiekofer,S., Kanitz,M., Klevesath,M.S., Joswig,M., Lee,V., Morcos,M., Tritschler,H., Ziegler,R., Wahl,P. *et al.* (1998) Insufficient glycemic control increases nuclear factor-kappa B binding activity in peripheral blood mononuclear cells isolated from patients with type 1 diabetes. *Diabetes Care.*, **21**, 1310–1316.
25. Bierhaus,A., Schiekofer,S., Schwaninger,M., Andrassy,M., Humpert,P.M., Chen,J., Hong,M., Luther,T., Henle,T., Kloting,I. *et al.* (2001) Diabetes-associated sustained activation of the transcription factor nuclear factor-kappaB. *Diabetes*, **50**, 2792–2808.
26. Zhou,W., Otto,E.A., Cluckey,A., Airik,R., Hurd,T.W., Chaki,M., Diaz,K., Lach,F.P., Bennett,G.R., Gee,H.Y. *et al.* (2012) FAN1 mutations cause karyomegalic interstitial nephritis, linking chronic kidney failure to defective DNA damage repair. *Nat. Genet.*, **44**, 910–915.
27. Constien,R., Forde,A., Liliensiek,B., Grone,H.J., Nawroth,P., Hammerling,G. and Arnold,B. (2001) Characterization of a novel EGFP reporter mouse to monitor Cre recombination as demonstrated by a Tie2 Cre mouse line. *Genesis*, **30**, 36–44.
28. Bolte,S. and Cordelieres,F.P. (2006) A guided tour into subcellular colocalization analysis in light microscopy. *J. Microsc.*, **224**, 213–232.
29. Manders,E.M.M., Verbeek,F.J. and Aten,J.A. (1993) Measurement of co-localization of objects in dual-colour confocal images. *J. Microsc.*, **169**, 375–382.
30. Dunn,K.W., Kamocka,M.M. and McDonald,J.H. (2011) A practical guide to evaluating colocalization in biological microscopy. *Am. J. Physiol. Cell Physiol.*, **300**, C723–C742.
31. Branzei,D. and Foiani,M. (2007) Interplay of replication checkpoints and repair proteins at stalled replication forks. *DNA Repair (Amst.)*, **6**, 994–1003.
32. Shapiro,R., Cohen,B.I., Shiuey,S.J. and Maurer,H. (1969) On the reaction of guanine with glyoxal, pyruvaldehyde, and kethoxal, and the structure of the acylguanines. A new synthesis of N2-alkylguanines. *Biochemistry*, **8**, 238–245.
33. Tsai,K.Y.F., Tullis,B., Breithaupt,K.L., Fowers,R., Jones,N., Grajeda,S., Reynolds,P.R. and Arroyo,J.A. (2021) A role for RAGE in DNA double strand breaks (DSBs) detected in pathological placentas and trophoblast cells. *Cells*, **10**, 857.
34. Kilic,S., Lezaja,A., Gatti,M., Bianco,E., Michelena,J., Imhof,R. and Altmeyer,M. (2019) Phase separation of 53BP1 determines liquid-like behavior of DNA repair compartments. *EMBO J.*, **38**, e101379.
35. Spegg,V. and Altmeyer,M. (2021) Biomolecular condensates at sites of DNA damage: more than just a phase. *DNA Repair (Amst.)*, **106**, 103179.
36. Pike,J.A., Styles,I.B., Rappoport,J.Z. and Heath,J.K. (2017) Quantifying receptor trafficking and colocalization with confocal microscopy. *Methods*, **115**, 42–54.
37. Harrigan,J.A., Belotserkovskaya,R., Coates,J., Dimitrova,D.S., Polo,S.E., Bradshaw,C.R., Fraser,P. and Jackson,S.P. (2011) Replication stress induces 53BP1-containing OPT domains in G1 cells. *J. Cell Biol.*, **193**, 97–108.
38. Ibarra,A., Schwob,E. and Mendez,J. (2008) Excess MCM proteins protect human cells from replicative stress by licensing backup origins of replication. *Proc. Natl. Acad. Sci. U. S. A.*, **105**, 8956–8961.
39. Pellettieri,J. and Sanchez Alvarado,A. (2007) Cell turnover and adult tissue homeostasis: from humans to planarians. *Annu. Rev. Genet.*, **41**, 83–105.
40. Ogrodnik,M., Salmonowicz,H. and Gladyshev,V.N. (2019) Integrating cellular senescence with the concept of damage accumulation in aging: relevance for clearance of senescent cells. *Aging Cell*, **18**, e12841.
41. Isnard,P., Rabant,M., Labaye,J., Antignac,C., Knebelmann,B. and Zaidan,M. (2016) Karyomegalic interstitial nephritis: a case report and review of the literature. *Medicine (Baltimore).*, **95**, e3349.
42. Maaroufi,K., Zakhama,A., Baudrimont,I., Achour,A., Abid,S., Ellouz,F., Dhouib,S., Creppy,E.E. and Bacha,H. (1999) Karyomegaly of tubular cells as early stage marker of the nephrotoxicity induced by ochratoxin A in rats. *Hum. Exp. Toxicol.*, **18**, 410–415.
43. Bierhaus,A., Fleming,T., Stoyanov,S., Leffler,A., Babes,A., Neacsu,C., Sauer,S.K., Eberhardt,M., Schnolzer,M., Lasitschka,F. *et al.* (2012) Methylglyoxal modification of Nav1.8 facilitates nociceptive neuron firing and causes hyperalgesia in diabetic neuropathy. *Nat. Med.*, **18**, 926–933.
44. Mulderrig,L., Garaycoechea,J.I., Tuong,Z.K., Millington,C.L., Dingler,F.A., Ferdinand,J.R., Gaul,L., Tadross,J.A., Arends,M.J., O'Rahilly,S. *et al.* (2021) Aldehyde-driven transcriptional stress triggers an anorexic DNA damage response. *Nature*, **600**, 158–163.
45. Li,T., Wei,Y., Qu,M., Mou,L., Miao,J., Xi,M., Liu,Y. and He,R. (2021) Formaldehyde and de/methylation in age-related cognitive impairment. *Genes (Basel)*, **12**, 913.
46. Kumar,V. and Nawroth,P.P. (2021) Is the association between diabetes mellitus and pulmonary fibrosis real? *Nat. Rev. Endocrinol.*, **17**, 703–704.
47. Kopf,S., Kumar,V., Kender,Z., Han,Z., Fleming,T., Herzig,S. and Nawroth,P.P. (2021) Diabetic pneumopathy - a new diabetes-associated complication: mechanisms, consequences and treatment considerations. *Front. Endocrinol. (Lausanne)*, **12**, 765201.
48. Saraiva,M.A., Borges,C.M. and Florencio,M.H. (2006) Reactions of a modified lysine with aldehydic and diketonic dicarbonyl compounds: an electrospray mass spectrometry structure/activity study. *J. Mass Spectrom.*, **41**, 216–228.
49. Oikonomou,D., Groener,J.B., Cheko,R., Kender,Z., Kihm,L., Fleming,T., Kopf,S. and Nawroth,P.P. (2018) Genetic polymorphisms of antioxidant and antiglycation enzymes and diabetic complications. How much can we learn from the genes? *Exp. Clin. Endocrinol. Diabetes*, **126**, 7–13.
50. Groener,J.B., Oikonomou,D., Cheko,R., Kender,Z., Zemva,J., Kihm,L., Muckenthaler,M., Peters,V., Fleming,T., Kopf,S. *et al.* (2019) Methylglyoxal and advanced glycation end products in patients with diabetes - what we know so far and the missing links. *Exp. Clin. Endocrinol. Diabetes*, **127**, 497–504.
51. Misono,S., Mizuno,K., Suetsugu,T., Tanigawa,K., Nohata,N., Uchida,A., Sanada,H., Okada,R., Moriya,S., Inoue,H. *et al.* (2021) Molecular signature of small cell lung cancer after treatment failure: the MCM complex as therapeutic target. *Cancers (Basel)*, **13**, 1187.
52. Kowal,T.J. and Falk,M.M. (2015) Primary cilia found on HeLa and other cancer cells. *Cell Biol. Int.*, **39**, 1341–1347.
53. Stead,B.E., Brandl,C.J., Sandre,M.K. and Davey,M.J. (2012) Mcm2 phosphorylation and the response to replicative stress. *BMC Genet.*, **13**, 36.
54. Xing,M., Wang,X., Palmai-Pallag,T., Shen,H., Helleday,T., Hickson,I.D. and Ying,S. (2015) Acute MUS81 depletion leads to replication fork slowing and a constitutive DNA damage response. *Oncotarget*, **6**, 37638–37646.
55. Kai,M., Boddy,M.N., Russell,P. and Wang,T.S. (2005) Replication checkpoint kinase Cds1 regulates Mus81 to preserve genome integrity during replication stress. *Genes Dev.*, **19**, 919–932.

56. Chuang,C.H., Wallace,M.D., Abratte,C., Southard,T. and Schimenti,J.C. (2010) Incremental genetic perturbations to MCM2–7 expression and subcellular distribution reveal exquisite sensitivity of mice to DNA replication stress. *PLos Genet.*, **6**, e1001110.
57. Mirman,Z. and de Lange,T. (2020) 53BP1: a DSB escort. *Genes Dev.*, **34**, 7–23.
58. Flynn,R.L. and Zou,L. (2011) ATR: a master conductor of cellular responses to DNA replication stress. *Trends Biochem. Sci*, **36**, 133–140.
59. Somyajit,K., Gupta,R., Sedlackova,H., Neelsen,K.J., Ochs,F., Rask,M.B., Choudhary,C. and Lukas,J. (2017) Redox-sensitive alteration of replisome architecture safeguards genome integrity. *Science*, **358**, 797–802.
60. Kunkel,T.A. (2003) Considering the cancer consequences of altered DNA polymerase function. *Cancer Cell*, **3**, 105–110.
61. Barbari,S.R. and Shcherbakova,P.V. (2017) Replicative DNA polymerase defects in human cancers: consequences, mechanisms, and implications for therapy. *DNA Repair (Amst.)*, **56**, 16–25.
62. Garcia,C.K. (2018) Insights from human genetic studies of lung and organ fibrosis. *J. Clin. Invest.*, **128**, 36–44.
63. Rodier,F., Coppe,J.P., Patil,C.K., Hoeijmakers,W.A., Munoz,D.P., Raza,S.R., Freund,A., Campeau,E., Davalos,A.R. and Campisi,J. (2009) Persistent DNA damage signalling triggers senescence-associated inflammatory cytokine secretion. *Nat. Cell Biol.*, **11**, 973–979.
64. Hatch,E.M., Fischer,A.H., Deerinck,T.J. and Hetzer,M.W. (2013) Catastrophic nuclear envelope collapse in cancer cell micronuclei. *Cell*, **154**, 47–60.
65. Working Group "In vitro micronucleus test", G.f.U.-M., Hintzsche,H., Hemmann,U., Poth,A., Utesch,D., Lott,J. and Stopper,H. (2017) Fate of micronuclei and micronucleated cells. *Mutat. Res. Rev. Mutat. Res.*, **771**, 85–98.
66. Utani,K., Kohno,Y., Okamoto,A. and Shimizu,N. (2010) Emergence of micronuclei and their effects on the fate of cells under replication stress. *PLoS One*, **5**, e10089.
67. Kwon,M., Leibowitz,M.L. and Lee,J.H. (2020) Small but mighty: the causes and consequences of micronucleus rupture. *Exp. Mol. Med.*, **52**, 1777–1786.
68. Leclerc,E., Fritz,G., Vetter,S.W. and Heizmann,C.W. (2009) Binding of S100 proteins to RAGE: an update. *Biochim. Biophys. Acta*, **1793**, 993–1007.
69. Gorsler,T., Murzik,U., Ulbricht,T., Hentschel,J., Hemmerich,P. and Melle,C. (2010) DNA damage-induced translocation of S100A11 into the nucleus regulates cell proliferation. *BMC Cell Biol.*, **11**, 100.
70. Pusterla,T., de Marchis,F., Palumbo,R. and Bianchi,M.E. (2009) High mobility group B2 is secreted by myeloid cells and has mitogenic and chemoattractant activities similar to high mobility group B1. *Autoimmunity*, **42**, 308–310.
71. Ramasamy,R., Yan,S.F. and Schmidt,A.M. (2011) Receptor for AGE (RAGE): signaling mechanisms in the pathogenesis of diabetes and its complications. *Ann. N.Y. Acad. Sci.*, **1243**, 88–102.
72. Qiu,S., Jiang,G., Cao,L. and Huang,J. (2021) Replication fork reversal and protection. *Front. Cell Dev. Biol.*, **9**, 670392.
73. Liliensiek,B., Weigand,M.A., Bierhaus,A., Nicklas,W., Kasper,M., Hofer,S., Plachky,J., Grone,H.J., Kurschus,F.C., Schmidt,A.M. *et al.* (2004) Receptor for advanced glycation end products (RAGE) regulates sepsis but not the adaptive immune response. *J. Clin. Invest.*, **113**, 1641–1650.
74. Bierhaus,A. and Nawroth,P.P. (2009) Multiple levels of regulation determine the role of the receptor for AGE (RAGE) as common soil in inflammation, immune responses and diabetes mellitus and its complications. *Diabetologia*, **52**, 2251–2263.
75. Frommhold,D., Kamphues,A., Hepper,I., Pruenster,M., Lukic,I.K., Socher,I., Zablotskaya,V., Buschmann,K., Lange-Sperandio,B., Schymeinsky,J. *et al.* (2010) RAGE and ICAM-1 cooperate in mediating leukocyte recruitment during acute inflammation in vivo. *Blood*, **116**, 841–849.
76. Bierhaus,A., Haslbeck,K.M., Humpert,P.M., Liliensiek,B., Dehmer,T., Morcos,M., Sayed,A.A., Andrassy,M., Schiekofer,S., Schneider,J.G. *et al.* (2004) Loss of pain perception in diabetes is dependent on a receptor of the immunoglobulin superfamily. *J. Clin. Invest.*, **114**, 1741–1751.
77. Sparvero,L.J., Asafu-Adjei,D., Kang,R., Tang,D., Amin,N., Im,J., Rutledge,R., Lin,B., Amoscato,A.A., Zeh,H.J. *et al.* (2009) RAGE (Receptor for Advanced Glycation Endproducts), RAGE ligands, and their role in cancer and inflammation. *J. Transl. Med.*, **7**, 17.
78. Chavakis,T., Bierhaus,A. and Nawroth,P.P. (2004) RAGE (receptor for advanced glycation end products): a central player in the inflammatory response. *Microbes Infect.*, **6**, 1219–1225.
79. Monferran,S., Paupert,J., Dauvillier,S., Salles,B. and Muller,C. (2004) The membrane form of the DNA repair protein Ku interacts at the cell surface with metalloproteinase 9. *EMBO J.*, **23**, 3758–3768.
80. Li,T., Diner,B.A., Chen,J. and Cristea,I.M. (2012) Acetylation modulates cellular distribution and DNA sensing ability of interferon-inducible protein IFI16. *Proc. Natl. Acad. Sci. U.S.A.*, **109**, 10558–10563.
81. Malewicz,M., Kadkhodaei,B., Kee,N., Volakakis,N., Hellman,U., Viktorsson,K., Leung,C.Y., Chen,B., Lewensohn,R., van Gent,D.C. *et al.* (2011) Essential role for DNA-PK-mediated phosphorylation of NR4A nuclear orphan receptors in DNA double-strand break repair. *Genes Dev.*, **25**, 2031–2040.
82. Ruzankina,Y., Pinzon-Guzman,C., Asare,A., Ong,T., Pontano,L., Cotsarelis,G., Zediak,V.P., Velez,M., Bhandoola,A. and Brown,E.J. (2007) Deletion of the developmentally essential gene ATR in adult mice leads to age-related phenotypes and stem cell loss. *Cell Stem Cell*, **1**, 113–126.
83. de Klein,A., Muijtjens,M., van Os,R., Verhoeven,Y., Smit,B., Carr,A.M., Lehmann,A.R. and Hoeijmakers,J.H. (2000) Targeted disruption of the cell-cycle checkpoint gene ATR leads to early embryonic lethality in mice. *Curr. Biol.*, **10**, 479–482.
84. Dendouga,N., Gao,H., Moechars,D., Janicot,M., Vialard,J. and McGowan,C.H. (2005) Disruption of murine Mus81 increases genomic instability and DNA damage sensitivity but does not promote tumorigenesis. *Mol. Cell. Biol.*, **25**, 7569–7579.
85. Slaats,G.G., Saldivar,J.C., Bacal,J., Zeman,M.K., Kile,A.C., Hynes,A.M., Srivastava,S., Nazmutdinova,J., den Ouden,K., Zagers,M.S. *et al.* (2015) DNA replication stress underlies renal phenotypes in CEP290-associated Joubert syndrome. *J. Clin. Invest.*, **125**, 3657–3666.